

1 **Heterogeneity and chemical reactivity of the remote troposphere defined by aircraft**
2 **measurements - Corrected**

3 Hao Guo¹, Clare M. Flynn², Michael J. Prather¹, Sarah A. Strode³, Stephen D. Steenrod³,
4 Louisa Emmons⁴, Forrest Lacey^{4,5}, Jean-Francois Lamarque⁴, Arlene M. Fiore⁶, Gus
5 Correa⁶, Lee T. Murray⁷, Glenn M. Wolfe^{3,8}, Jason M. St. Clair^{3,8}, Michelle Kim⁹, John
6 Crouse¹⁰, Glenn Diskin¹⁰, Joshua DiGangi¹⁰, Bruce C. Daube^{11,12}, Roisin Commane^{11,12},
7 Kathryn McKain^{13,14}, Jeff Peischl^{14,15}, Thomas B. Ryerson^{13,15}, Chelsea Thompson¹³,
8 Thomas F. Hanisco³, Donald Blake¹⁶, Nicola J. Blake¹⁶, Eric C. Apel⁴, Rebecca S.
9 Hornbrook⁴, James W. Elkins¹⁴, Eric J. Hintsa^{13,14}, Fred L. Moore^{13,14}, Steven Wofsy¹¹

10 ¹ Department of Earth System Science, University of California, Irvine, CA 92697

11 ² Department of Meteorology, Stockholm University, Stockholm SE-106 91, Sweden

12 ³ Atmospheric Chemistry and Dynamics Laboratory, NASA Goddard Space Flight
13 Center, Greenbelt, MD 20771

14 ⁴ Atmospheric Chemistry Observations and Modeling Laboratory, National Center for
15 Atmospheric Research, Boulder, CO 80301

16 ⁵ Department of Mechanical Engineering, University of Colorado, Boulder, CO 80309

17 ⁶ Department of Earth and Environmental Sciences and Lamont-Doherty Earth
18 Observatory, Columbia University, Palisades, NY 10964

19 ⁷ Department of Earth and Environmental Sciences, University of Rochester, Rochester,
20 NY 14611

21 ⁸ Joint Center for Earth Systems Technology, University of Maryland, Baltimore County,
22 Baltimore, MD 21228

23 ⁹ Department of Geological and Planetary Sciences, California Institute of Technology,
24 Pasadena, CA 91125

25 ¹⁰ Atmospheric Composition, NASA Langley Research Center, Hampton VA 23666

26 ¹¹ John A. Paulson School of Engineering and Applied Sciences, Harvard University,
27 Cambridge, MA 02138

28 ¹² Department of Earth and Planetary Sciences, Harvard University, Cambridge, MA
29 02138

30 ¹³ Cooperative Institute for Research in Environmental Sciences, University of Colorado,
31 Boulder, CO 80309

32 ¹⁴ Global Monitoring Division, Earth System Research Laboratory, NOAA, Boulder, CO
33 80305

34 ¹⁵ Chemical Sciences Division, National Oceanic and Atmospheric Administration Earth
35 System Research Laboratory, Boulder, CO 80305

36 ¹⁶ Department of Chemistry, University of California, Irvine, CA 92697

37
38 *Correspondence to:* Hao Guo (haog2@uci.edu) and Michael J. Prather
39 (mprather@uci.edu).
40

41 **Keywords:** Tropospheric Chemistry, Ozone, Methane, Aircraft Observations, NASA
42 ATom

43 **Abstract.** The NASA Atmospheric Tomography (ATom) mission built a photochemical
44 climatology of air parcels based on in situ measurements with the NASA DC-8 aircraft
45 along objectively planned profiling transects through the middle of the Pacific and
46 Atlantic oceans. In this paper we present and analyze a data set of 10 s (2 km) merged
47 and gap-filled observations of the key reactive species driving the chemical budgets of O₃
48 and CH₄ (O₃, CH₄, CO, H₂O, HCHO, H₂O₂, CH₃OOH, C₂H₆, higher alkanes, alkenes,
49 aromatics, NO_x, HNO₃, HNO₄, peroxyacetyl nitrate, other organic nitrates), consisting of
50 146,494 distinct air parcels from ATom deployments 1 through 4. Six models calculated
51 the O₃ and CH₄ photochemical tendencies from this modeling data stream for ATom 1.
52 We find that 80 % – 90 % of the total reactivity lies in the top 50 % of the parcels; and 25
53 % – 35 %, in the top 10 %, supporting previous model-only studies that tropospheric
54 chemistry is driven by a fraction of all the air. Surprisingly, the probability densities of
55 species and reactivities averaged on a model scale (100 km) differ only slightly from the
56 2 km ATom 10 s data, indicating that much of the heterogeneity in tropospheric
57 chemistry can be captured with current global chemistry models. Comparing the ATom
58 reactivities over the tropical oceans with climatological statistics from six global
59 chemistry models, we find generally good agreement with the reactivity rates for O₃ and
60 CH₄. Models distinctly underestimate O₃ production below 2 km relative to the mid-
61 troposphere, and this can be traced to lower NO_x levels than observed. Attaching
62 photochemical reactivities to measurements of chemical species allows for a richer, yet
63 more constrained-to-what-matters, set of metrics for model evaluation.

64

65

66 **Preface.** This paper presents a corrected version of the paper published under the same
67 authors and title (sans 'Corrected') as <https://doi.org/10.5194/acp-21-13729-2021>. While
68 continuing our analysis of the ATom data we found several major mistakes or decision
69 errors. The main conclusions were unchanged except those regarding production of O₃,
70 but most of the numbers and many of the figures changed slightly. A corrigendum to the
71 original 2021 paper was prepared, but the changes were extensive enough so that the
72 ACP editors and the authors decided that a completely new paper should be produced and
73 the 2021 paper withdrawn. The errors that were corrected are described in this preface
74 and discussed at most briefly in the paper. First, we found that measurement errors in
75 PAN and HNO₄ were large (~100 ppt), and when this occurred in the lower troposphere,
76 the rapid thermal decomposition released large amounts of NO_x. There is no easy fix for
77 this, and we developed a new protocol (RDS*) for computing reactivities by allowing the
78 species to thermally decompose before use in the model, as described below. This fix
79 greatly reduced O₃ production (P-O3) in the lower troposphere. A second NO_x problem
80 involved the propagation of polluted profiles from the Los Angeles basin to gap filling
81 over the tropical eastern Pacific. This correction resulted in the update of the Modeling
82 Data Stream to version 2b. These NO_x errors cause noticeable changes in reactivities,
83 especially P-O3. Other decision errors led us to decrease the southern latitude extent of
84 the Atlantic and Pacific transects from 54° S to 53° S to avoid spurious parcels being
85 included. Also, cosine of latitude weighting was applied to data for all figures and tables.
86 The UCI model now includes all higher alkanes and alkenes in the ATom data as C₃H₈
87 and C₂H₄, respectively. These last three decision errors had detectable but small impacts.

88

89 The most worrisome error was the evolution of the UCI CTM model's ATom version
 90 from its use in the MDS-0 results shown here to the final calculations with MDS-2 as the
 91 UCI2* model in the 2021 paper. The first MDS-0 UCI model was taken directly from
 92 the main CTM code line and developed for Prather et al. (2017; 2018) by Xin Zhu (not on
 93 the 2021 paper). This model was then further adapted and developed for the 2021 paper
 94 and for additional complex sensitivity tests. At this stage (i.e., the UCI2* simulations in
 95 the 2021 paper), the results failed several logic tests and were irreproducible. With the
 96 decision to withdraw the paper, we returned to the MDS-0 UCI model, and Xin Zhu
 97 adapted it to more efficient ATom runs as well as adding several new diagnostics and
 98 checks to ascertain the ATom runs were being calculated correctly. As noted in the paper
 99 below, we carefully checked the O₃ budget in terms of rates and tendencies, and these are
 100 now consistent in model UCIZ. Further, the sensitivity coefficients ($\partial \ln R / \partial \ln X$ and
 101 $\partial^2 \ln R / \partial \ln X \partial \ln Y$) calculated for a subsequent paper are now closer to theoretical
 102 expectations for a quasi-linear system. The UCIZ* model results here are our best,
 103 revised estimate of the ATom reactivities.

104

105

106 1 Prologue

107

108 This paper is based on the methods and results of papers that established an approach for
 109 analyzing aircraft measurements, specifically the NASA Atmospheric Tomography
 110 Mission (ATom), with global chemistry models. Here we present a brief overview of
 111 those papers to help the reader understand the basis for this paper. The first ATom
 112 modeling paper ("Global atmospheric chemistry – which air matters", Prather et al., 2017,
 113 hence P2017) gathered six global models, both chemistry-transport models (CTMs) and
 114 chemistry-climate models (CCMs). The models reported a single-day snapshot for mid-
 115 August (the time of the first ATom deployment, ATom-1), and these included all species
 116 relevant for tropospheric chemistry and the 24 h reactivities. We limited our study to
 117 three reactivities (Rs) controlling methane (CH₄) and tropospheric ozone (O₃) using
 118 specific reaction rates to define the loss of CH₄ and the production and loss of O₃ in parts
 119 per billion (ppb) per day. The critical photolysis rates (*J* values) were also reported as 24
 120 h averages.

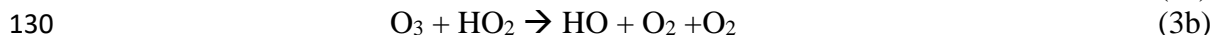
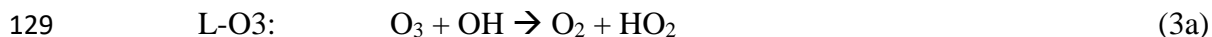
121



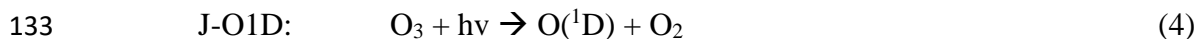
123



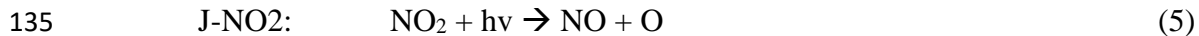
128



132



134



138 Models also reported the change in O_3 over 24 h, and these match the P-O3 minus L-O3
139 values over the Pacific basin (a focus of this study). The models showed a wide range in
140 the three Rs average profiles across latitudes over the Pacific basin, as well as 2D
141 probability densities (PDs) for key species such as NO_x ($\text{NO} + \text{NO}_2$) versus HOOH. A
142 large part of the model differences was attributed to the large differences found in
143 chemical composition rather than the calculation of rates from that composition. We
144 found that single transects from a model through the tropical Pacific at different
145 longitudes produced nearly identical 2D PDs, but these PDs were distinctly different
146 across models. This result supported the premise that the ATom PDs would provide a
147 useful metric for global chemistry models.
148

149 In P2017, we established a method for running the chemistry modules in the CTMs and
150 CCMs with an imposed chemical composition from aircraft data: the ATom run, or “A
151 run”. In the A run, the chemistry of each grid cell does not interact with its neighbors or
152 with externally imposed emission sources. Effectively the CTM/CCM is initialized and
153 run for 24 h without transport, scavenging or emissions. Aerosol chemistry is also turned
154 off in the A runs. This method allows each parcel to evolve in response to the daily cycle
155 of photolysis in each model and be assigned a 24 h integrated reactivity. The
156 instantaneous reaction rates at the time an air parcel is measured (e.g., near sunset at the
157 end of a flight) do not reflect that parcel's overall contribution to the CH_4 or O_3 budget; a
158 full diel cycle is needed. The A run assumption that parcels do not mix with neighboring
159 air masses is an approximation, and thus for each model we compared the A runs using
160 the model's restart data with a parallel standard 24 h simulation (including transport,
161 scavenging, and emissions). Because the standard grid-cell air moves and mixes, we
162 compared averages over a large region (e.g., tropical Pacific). We find some average
163 biases of order $\pm 10\%$ but general agreement. The largest systematic biases in the A runs
164 are caused by buildup of HOOH (no scavenging) and decay of NO_x (no sources). The A
165 runs are relatively easy to code for most CTM/CCMs and allow each model's chemistry
166 module, including photolysis package, to run normally. The A runs do not distinguish
167 between CTMs and CCMs, except that each model will generate/prescribe its own cloud
168 fields and photolysis rates. Our goal is to create a robust understanding of the chemical
169 statistics including the reactivities with which to test and evaluate the free-running
170 CCMs, and thus we do not try to model the specific period of the ATom deployments.
171 Others may use the ATom data with hindcast CTMs to test forecast models, but here we
172 want to build a chemical climatology.
173

174 The first hard test of the A runs came with the second ATom modeling paper ("How well
175 can global chemistry models calculate the reactivity of short-lived greenhouse gases in
176 the remote troposphere, knowing the chemical composition", Prather et al., 2018, hence
177 P2018). The UCI CTM simulated an aircraft-like data set of 14,880 air parcels along the
178 International Date Line from a separate high-resolution (0.5°) model. Each parcel is
179 defined by the following core species: H_2O , O_3 , NO_x , HNO_3 , HNO_4 , PAN (peroxyacetyl
180 nitrate), CH_3NO_3 , HOOH, CH_3OOH , HCHO, CH_3CHO (acetaldehyde), $\text{C}_3\text{H}_6\text{O}$ (acetone),

181 CO, CH₄, C₂H₆, alkanes (C₃H₈ and higher), C₂H₄, aromatics (benzene, toluene, xylene)
182 and C₅H₈ (isoprene), plus temperature. Short-lived radicals (e.g., OH, HO₂, CH₃OO)
183 were initialized at small concentrations and quickly reached daytime values determined
184 by the core species. The six CTM/CCMs overwrote the chemical composition of a restart
185 file, placing each pseudo-observation in a unique grid cell according to its latitude,
186 longitude, and pressure. If another parcel is already in that cell, then it is shifted east–
187 west or north–south to a neighboring model cell. For coarse-resolution models, multiple
188 restart files and A runs were used to avoid large location shifts. CTM/CCMs usually
189 have a locked in 24 h integration step starting at 0000 UTC that is extremely difficult to
190 modify in order to try to match the local solar time of observation, especially as it
191 changes along aircraft flights. We tested the results with a recoded UCI CTM to start at
192 1200 UTC but retain the same clouds fields over the day and found only percentage-level
193 differences between a midnight or noon start.

194

195 These A runs averaged over cloud conditions by simulating 5 d in August at least 5 d
196 apart. Assessment of the modeled photolysis rates and comparison with the ATom-
197 measured *J* values is presented in Hall et al. (2018, hence H2018). All models agreed
198 that a small fraction of chemically hot air parcels in the synthetic data set controlled most
199 of the total reactivity. Some models had difficulty in implementing the A runs because
200 they overwrote the specified water vapor with the modeled value, but this problem is
201 fixed here. In both P2017 and P2018, the GISS-E2 model stood out with the most
202 unusual chemistry patterns and sometimes illogical correlations. Efforts by a co-author
203 to clarify the GISS results or identify errors in the implementation have not been
204 successful. GISS results are included here for completeness in the set of three papers but
205 are not reconciled. Overall, three models showed remarkable inter-model agreement in
206 the three Rs with less than half of the RMSD (root-mean-square difference) as compared
207 with the other models. UCI also tested the effect of different model years (1997 and
208 2015 versus reference year 2016), which varies the cloud cover and photolysis rates, and
209 found an inter-year RMSD about half of that of the core model’s RMSD. Thus, there is a
210 fundamental uncertainty in this approach due to the inability to specify the
211 cloud/photolysis history seen by a parcel over 24 h, but it is less than the inter-model
212 differences among the most similar models.

213

214 **2 Introduction**

215

216 The NASA Atmospheric Tomography (ATom) mission completed a four-season
217 deployment, each deployment flying from the Arctic to Antarctic and back, traveling
218 south through the middle of the Pacific Ocean, across the Southern Ocean and then north
219 through the Atlantic Ocean, with near-constant profiling of the marine troposphere from
220 0.2 to 12 km altitude (see Fig. S1). The DC8 was equipped with in situ instruments that
221 documented the chemical composition and conditions at time intervals ranging from <1
222 to about 100 seconds (Wofsy et al., 2018). ATom measured hundreds of gases and
223 aerosols, providing information on the chemical patterns and reactivity in the vast remote
224 ocean basins, where most of the destruction of tropospheric ozone (O₃) and methane
225 (CH₄) occurs. Reactivity is defined here as in P2017 to include the production and loss
226 of O₃ (P-O3 and L-O3, ppb/d) and loss of CH₄ (L-CH4, ppb/d). Here we report on this

227 model-derived product that was proposed for ATom, the daily averaged reaction rates
228 determining the production and loss of O₃ and the loss of CH₄ for 10 s averaged air
229 parcels. We calculate these rates with 3D chemical models that include variations in
230 clouds and photolysis, and then assemble the statistical patterns describing the
231 heterogeneity (i.e., high spatial variability) of these rates and the underlying patterns of
232 reactive gases.

233 Tropospheric O₃ and CH₄ contribute to climate warming and global air pollution (Stocker
234 et al., 2013). Their abundances in the troposphere are controlled largely by tropospheric
235 chemical reactions. Thus, chemistry–climate assessments seeking to understand past
236 global change and make future projections for these greenhouse gases have focused on
237 the average tropospheric rates of production and loss and how these reactivities are
238 distributed in large semi-hemispheric zones throughout the troposphere (Griffiths et al.,
239 2021; Myhre et al., 2014; Naik et al., 2013; Prather et al., 2001; Stevenson, et al., 2006;
240 Stevenson, et al., 2013; Stevenson, et al., 2020; Voulgarakis et al., 2013; Young et al.,
241 2013). The models used in these assessments disagree on these overall CH₄ and O₃
242 reactivities (a.k.a. the budgets), and resolving the cause of such differences is stymied
243 because of the large number of processes involved and the resulting highly heterogeneous
244 distribution of chemical species that drive the reactions. Simply put, the models use
245 emissions, photochemistry, and meteorological data to generate the distribution of key
246 species such as nitrogen oxides (NO_x = NO + NO₂) and hydrogen peroxide (HOOH)
247 (step 1) and then calculate the CH₄ and O₃ reactivities from these species (step 2). There
248 is no single average measurement that can test the verisimilitude of the models.
249 Stratospheric studies such as Douglass et al. (1999) have provided a quantitative basis for
250 testing chemistry and transport, and defining model errors; but few of these studies have
251 tackled the problem of modeling the heterogeneity of tropospheric chemistry. The major
252 model differences lie in the first step, because when we specify the mix of key chemical
253 species, most models agree on the CH₄ and O₃ chemical budgets (*P2018*). The intent of
254 ATom was to collect an atmospheric sampling of all the key species and the statistics
255 defining their spatial variability, and thus that of the reactivities of CH₄ and O₃.

256 Many studies have explored the ability of chemistry–transport models (CTMs) to resolve
257 finer scales such as pollution layers (Eastham and Jacob, 2017; Rastigejev et al., 2010;
258 Tie et al., 2010; Young et al., 2018; Zhuang et al., 2018), but these have not had the
259 chemical observations (statistics) to evaluate model performance. In a great use of
260 chemical statistics, Yu et al. (2016) used 60 s data (~12 km) from the SEAC⁴RS aircraft
261 mission to compare cumulative probability densities (PDs) of NO_x, O₃, HCHO and
262 isoprene over the Southeast US with the GEOS-Chem CTM run at different resolutions.
263 They identified clear biases at the high and low ends of the distribution, providing a new
264 test of models based on the statistics rather than mean values. Heald et al. (2011)
265 gathered high-resolution profiling of organic and sulfate aerosols from 17 aircraft
266 missions and calculated statistics (mean, median, quartiles) but only compared with the
267 modeled means. The HIAPER Pole-to-Pole Observations (HIPPO) aircraft mission
268 (Wofsy, 2011) was a precursor to ATom with regular profiling of the mid-Pacific
269 including high-frequency 10 s sampling that identified the small scales of variability
270 throughout the troposphere. HIPPO measurements were limited in species, lacking O₃,
271 NO_x and many of the core species needed for reactivity calculations. ATom, with a full

272 suite of reactive species and profiling through the Atlantic basin, provides a wealth of
273 chemical statistics that challenge the global chemistry models.

274 One main task here is the assembly of the modeling data stream (MDS), which provides
275 flight-wise continuous 10 s data (air parcels) for the key reactive species. The MDS is
276 based on direct observations and interpolation methods to fill gaps as documented the
277 Supplement. Using the version 0 of the MDS, we have six chemical models calculating
278 the 24 h reactivities, producing a reactivity data stream (RDS version 0) using protocols
279 noted in the Prologue (P2017) and described further in Sect. 3.2. There, we describe the
280 updated modeling protocol RDS* necessary to address measurement noise in PAN and
281 HNO₄, which can be very short-lived. In Sect. 4, we examine the statistics of reactivity
282 over the Atlantic and Pacific oceans, focusing on air parcels with high reactivity; for
283 example, 10% of the parcels produce 25-35% of total reactivity over the oceans. We
284 compare these ATom-1 statistics, species and reactivities with August climatologies from
285 six global chemistry models. In one surprising result, ATom-1 shows a more reactive
286 tropical troposphere than found in most models' climatologies associated with higher
287 NO_x levels than in the models. Section 5 concludes that the ATom PDs based on 10s air
288 parcels do provide a valid chemistry metric for global models with 1° resolution. It also
289 presents some examples where ATom measurements and modeling can test the chemical
290 relationships and may address the cause of differences in the O₃ and CH₄ budgets
291 currently seen across the models. With this paper we release the full ATom MDS-2b
292 from all four deployments along with the updated RDS-2b reactivities from the UCI
293 model.

294 **3 Models and data**

295 **3.1 The modeling data stream (MDS)**

296 The ATom mission was designed to collect a multi-species, detailed chemical
297 climatology that documents the spatial patterns of chemical heterogeneity throughout the
298 remote troposphere. Figure S1 in the Supplement maps the 48 research flights, and the
299 Supplement has tables summarizing each flight. We required a complete set of key
300 species in each air parcel to initialize the models that calculate the CH₄ and O₃
301 reactivities. We choose the key reactive species (H₂O, O₃, CO, CH₄, NO_x, NO_xPSS,
302 HNO₃, HNO₄, PAN, CH₂O, H₂O₂, CH₃OOH, acetone, acetaldehyde, C₂H₆, C₃H₈, *i*-
303 C₄H₁₀, *n*-C₄H₁₀, alkanes, C₂H₄, alkenes, C₂H₂, C₃H₈, benzene, toluene, xylene,
304 CH₃ONO₂, C₂H₅ONO₂, RONO₂, CH₃OH) directly from the ATom measurements and
305 then add corollary species or other observational data indicative of industrial or biomass
306 burning pollution or atmospheric processing (HCN, CH₃CN, SF₆, relative humidity,
307 aerosol surface area (four modes), and cloud indicator). We choose 10 s averages for our
308 air parcels as a compromise and because the 10 s merged data are a standard product
309 (Wofsy et al., 2018). A few instruments measure at 1 s intervals, but the variability at
310 this scale is not that different from 10 s averages (Fig. S2). Most of the key species are
311 reported as 10 s values, with some being averaged or sampled at 30 s or longer such as
312 ~90 s for some flask measurements.

313 Throughout ATom, gaps occur in individual species on a range of timescales due to
314 calibration cycles, sampling rates or instrument malfunction. The generation of the MDS

315 uses a range of methods to fill these gaps and assigns a flag index to each species and
316 data point to allow users to identify direct measurements and methods used for gap-
317 filling. Where two instruments measure the same species, the MDS selects a primary
318 measurement and identifies which instrument was used with a flag. The methodology
319 and species-specific information on how the current MDS version 2 (MDS-2) is
320 constructed, plus statistics on the 48 research flights and the 146,494 10 s air parcels in
321 MDS-2 are given in the Supplement.

322 Over the course of this study, several MDS versions were developed and tested, including
323 model-derived RDSs from these versions, some of which are used in this paper. In early
324 ATom science team meetings, there was concern about the accuracy of NO₂ direct
325 measurements when at very low concentrations. A group prepared an estimate for NO_x
326 using the NO and O₃ measurements to calculate a photostationary value for NO₂ and thus
327 NO_x. This PSS-NO_x became the primary NO_x source in version 0 (i.e., MDS-0). With
328 MDS-0, we chose to gap-fill using correlations with CO to estimate the variability of the
329 missing measurement over the gap. The science team then rejected PSS-NO_x as a proxy,
330 and we reverted to the observed NO + NO₂ resulting in NO_x values that are 25 % larger
331 on average than in MDS-0 (unweighted mean of 66 vs. 52 ppt). This change affected P-
332 O₃ most and L-CH₄ least. We then estimated errors in the gap-filling and found that CO
333 had little skill as a proxy for most other species. With MDS-2, we optimized and tested
334 the treatments of gap-filling and lower limit of detection, along with other quality
335 controls. With continued analysis of the unusually reactive East Pacific region, we
336 determined that the method of long-gap filling for NO_x resulted in propagation of high
337 NO_x levels from the over-land profiles into the over-water profiles in the tropics. We
338 separated these two set of profiles used for long-gap NO_x filling and created an updated
339 version 2b. This experience points to the importance of having reliable, continuous NO_x
340 measurements. MDS-2b is fully documented in the Supplementary Information.

341

342 **3.2 The reactivity data stream (RDS)**

343 The concept of using an MDS to initialize 3D global chemistry models and calculate an
344 RDS was developed in the pre-ATom methodology papers (P2017; P2018). In this
345 paper, we use the original six models for their August chemical statistics, and we use 5 of
346 them plus a box model to calculate the reactivities, see Table 1. The RDS is really a
347 protocol applied to the MDS. It is introduced in the Prologue and the details can be
348 found in P2018. A model grid cell chosen to be close to the measured parcel is initialized
349 with all the core reactive species needed for a regular chemistry simulation. The model is
350 then integrated over 24 h without transport or mixing, without scavenging, and without
351 emissions. Each global model uses its own varying cloud fields for the period to
352 calculate photolysis rates; but the F0AM box model simply takes the instant J-values as
353 measured on the flight and applies a diurnal scaling. We initialize with the core species
354 and let the radicals (OH, HO₂, RO₂) come quickly into photochemical balance. The 24 h
355 integration is not overly sensitive to the start time of the integration, and thus models do
356 not have to synchronize with the local time of observation (see P2018's Fig. S8 and Table
357 S8).

358 The initial ATom-1 reactivities came from MDS-0 and six of the models in Table 1.
359 Although these RDS-0 model results are now out of date because of the move to MDS-
360 2b, they provide critical information on how models agree, or disagree, in calculating the
361 RDS using the ATom protocol. Thus we include them here as a cross-model comparison.
362 Given the excellent agreement at the parcel level using three models (GC, GMI, UCI),
363 and with a desire to avoid wasting the community's time, we continued the analysis of
364 MDS-2b with just our local UCI CTM. This decision may need to be revisited.

365 Statistics for the three reactivities for six models using MDS-0 are given in Table 2 and
366 Table S8 for three domains: global (all points), Pacific (oceanic data from 53° S to 60° N)
367 and Atlantic (same constraints as Pacific). The statistics try to achieve equal latitude-by-
368 pressure sampling by weighting each ATom parcel inversely according to the number of
369 parcels in each 10° latitude by 100 hPa bin, and each point is also cosine(latitude)
370 weighted. We calculate the means and medians plus the percent of total reactivity in the
371 top 10 % of the weighted parcels (Table 2) and also the mean reactivity of the top 10 %,
372 percent of total reactivity in the top 50 %, 10 % and 3 % plus the mean *J* values (Table
373 S8).

374 These six-model version 0 statistics are shown alongside the version 2b results using the
375 current UCIZ model but with a new protocol designated RDS*. While investigating
376 sensitivities in the RDS, we found an inconsistency between the reported concentrations
377 of both pernitric acid (HNO₄) and peroxyacetyl nitrate (PAN) with respect to the
378 chemical kinetics used in the models. High concentrations (100 ppt, attributed to
379 instrument noise) were reported under conditions where the thermal decomposition
380 frequency was > 0.4 per hour in the lower troposphere (> 253 K for HNO₄ and > 291 K
381 for PAN). Thus, these species instantly become NO_x. While these measurements are
382 clearly spurious, there is no easy fix. We developed a new protocol, RDS*, that allows
383 both species to decay for 24 h using their local thermal decomposition rate before being
384 used in the model. This protocol avoids much of the fast thermal release of NO_x in the
385 lower atmosphere during the first 24 h of the RDS calculation, but does not affect the
386 release of NO_x from photolysis or OH reactions in the upper troposphere where thermal
387 decomposition is inconsequential. It is possible that some of the high concentrations of
388 HNO₄ and PAN in the lower troposphere are real and that we are missing this large
389 source of NO_x with the RDS* protocol, but we find no obvious sources of these species
390 in the remote oceanic regions that would produce enough to match the thermal loss. Both
391 this problem and its solution do not affect the initial NO_x values.

392
393 We present the RDS-2b reactivities calculated under the RDS* protocol with the UCI
394 CTM developed by Xin Zhu for P2017 and P2018 (designated UCIZ*) as our best results
395 in the final column of Tables 2 and S8. We added diagnostics that give us confidence in
396 our O₃ reactivities: the approximate P-O₃ and L-O₃ based on the limited reactions (rates
397 2abd and 3abc above) actually predict the calculated 24 h O₃ tendency, see Fig. S6.
398 Considering the ocean basin observations only, P-L ranges from -12 to +15 ppb/d. The
399 mean error in P-L is about -0.01 ppb/d, and the root-mean-squared error is about 0.04
400 ppb/d, convincing us that we have correctly diagnosed the P-O₃ and L-O₃ terms.
401 Following the practice of the GMI model, we also record the initial and 24-hour

402 abundances of all the ATom species to check that nothing unusual altered the species
403 abundance in each cell over the 24 hours.

404

405 **3.3 Inter-model differences**

406

407 Variations in reactivities due to clouds are an irreducible source of uncertainty:
408 predicting the cloud-driven photolysis rates that a shearing air parcel will experience over
409 24 h is not possible here. The protocol uses 5 separated 24 h days to average over
410 synoptically varying cloud conditions. The standard deviation (σ) of the 5 d, as a
411 percentage of the 5 d mean, is averaged over all parcels and shown in Table S9 for the
412 five global models. Three central models (GC, GMI, UCI) show 9 %–10 % $\sigma(J_s)$ values
413 and similar $\sigma(R_s)$ values as expected if the variation in J values is driving the reactivities.
414 Two models (GISS, NCAR) have 12 %–17 % $\sigma(J_s)$, which might be explained by more
415 opaque clouds, but the amplified $\sigma(R)$ values (14 %–32 %) are inexplicable. This
416 discrepancy needs to be resolved before using these two models for ATom RDS analysis.

417

418 Inter-model differences are shown in the parcel-by-parcel root-mean-square (rms)
419 differences for RDS-0 in Table 3. Even when models adopt standard kinetic rates and
420 cross sections (i.e., Burkholder et al., 2015), the number of species and chemical
421 mechanisms included, as well as the treatment of families of similar species or
422 intermediate short-lived reaction products, varies across models. For example, UCI
423 considers about 32 reactive gases, whereas GC and GMI have over 100, and FOAM has
424 more than 600. The other major difference across models is photolysis, with models
425 having different cloud data and different methods for calculating photolysis rates in
426 cloudy atmospheres (H2018). The three central models (GC, GMI, UCI) in terms of their
427 5 d variability (Table S9) are also most closely alike in these statistics with rms = 20 %–
428 30 % for L-CH₄ up to 26 %–35 % for P-O₃. These rms values appear to be about as
429 close as any two models can get. The intra-model rms for different years (UCI 2016
430 versus 1997) is 10 %–13 % and shows that we are seeing basic differences in the
431 chemical models across GC, GMI, and UCI. FOAM is the next closest to these central
432 models, but it will inherently have a larger rms because it is a 1 d calculation and not a 5
433 d average. NCAR's rms is consistently higher and likely related to what is seen in the 5 d
434 σ values in Table S9. GISS is clearly different from all the others (L-CH₄ rms > 100 %
435 while L-O₃ rms < 66 %).

436

437 **4 Results**

438

439 Our analysis of the reactivities uses the six-model RDS-0 results to examine the
440 consistency in calculating the R_s across models. Thereafter, we rely on the similar results
441 from the three central models (GC, GMI, UCI) to justify use of UCIZ* with MDS-2b as
442 our best estimate for ATom reactivities. The uncertainty in this estimate can be
443 approximated by the inter-model spread of the central models as discussed above. When
444 evaluating the model climatologies for chemical species, we use MDS-2b. A summary of
445 the key data files used here, as well as their sources and contents, is given in Table 4.

446

447 **4.1 Probability densities of the reactivities**

448

449 The reactivities for three large domains (Global, Pacific, Atlantic) from the six-model
450 RDS-0 are summarized in Tables 2 and S8. Sorted PDs for the three Rs and Pacific and
451 Atlantic Ocean basins are plotted in Fig. 1 and show the importance of the most reactive
452 “hot” parcels with deeply convex curves and the sharp upturn in R values above 0.9
453 cumulative weight (top 10 %). Both basins show a similar emphasis on the most reactive
454 hot parcels: 80 % – 90 % of total R is in the top 50 % of the parcels, 25 % – 35 % is in
455 the top 10 %, and about 10 % – 14 % is in the top 3 %. The corollary is that the bottom
456 50 % parcels control only 10 % – 20 % of the total reactivity, which is why the median is
457 less than mean (except for P-O3 in the Atlantic).

458

459 The enhancement factor for the top 50 % L-CH₄ parcels is 2.0 (84 % of reactivity in 42
460 % of mass) given that our 53 °S – 60 °N transects cover 83 % of the air mass below 200
461 hPa and assuming that L-CH₄ is negligible poleward of these transects. This
462 enhancement factor is a large-scale feature because the tropical lower troposphere, being
463 warm and wet with high sun, dominates the budget. It is seen in previous model
464 intercomparisons that calculate budgets in large tropospheric blocks like Voulgarakis et
465 al. (2013) with 63 % of L-CH₄ in 31 % of the air mass (500 hPa–surface, 30 °S – 30 °N).
466 The impact of the extremely hot parcels and the heterogeneity seen in the ATom 10 s
467 parcels is evident in the steep slopes above the 90th percentile, yielding enhancement
468 factors of 3 to 4.

469

470 Each R value and each ocean has a unique shape; for example L-O3 in the Atlantic is
471 almost two straight lines breaking at the 50th percentile. In Fig. 1 the agreement across
472 all models (except GISS) is clear, indicating that the conclusion in *P2018* (i.e., that most
473 global chemistry models agree on the O₃ and CH₄ budgets if given the chemical
474 composition) also holds for the ATom-measured chemical composition. Comparing the
475 brown (UCI, RDS-0) and black-dashed (UCIZ, RDS*-2) lines, we find that the shift from
476 MDS-0 to MDS-2b plus the new RDS* (HNO₄+PAN) protocol produces large reductions
477 in P-O3 for all cumulative weights and small reductions in L-CH₄ for the upper 5th
478 percentile. We conclude that accurate modeling of chemical composition of the 80th and
479 greater percentiles is important but that modest errors in the lowest 50th percentile are
480 inconsequential; effectively, some parcels matter more than others (P2017).

481

482 How well does this ATom analysis work as a model intercomparison project? Overall,
483 we find that most models give similar results when presented with the ATom-1 MDS.
484 The broad agreement of the cumulative reactive PDs across a range of model
485 formulations using differing levels of chemical complexity shows this approach is robust.
486 The different protocols for calculating reactivities as well as the uncertainty in cloud
487 fields appear to have a small impact on the shape of the cumulative PDs but are
488 informative regarding the minimum structural uncertainty in estimating the 24 h
489 reactivity of a well-measured air parcel.

490 **4.2 Spatial heterogeneity of tropospheric chemistry**

491 A critical unknown for tropospheric chemistry modeling is what resolution is needed to
492 correctly calculate the budgets of key gases. A similar question was addressed in Yu et

493 al. (2016) for the isoprene oxidation pathways using a model with variable resolution
494 (500 km, 250 km and 30 km) compared to aircraft measurements; see also ship plume
495 chemistry in Charlton-Perez et al. (2009). ATom's 10 s air parcels measure 2 km
496 (horizontal) by 80 m (vertical) during most profiles. There are obviously some chemical
497 structures below the 10 s air parcels. Only some ATom measurements are archived at 1
498 Hz, and we examine a test case using 1 s data for O₃ and H₂O for a mid-ocean descent
499 between Anchorage and Kona in Fig. S2a in the Supplement. Some of the 1 s (200 m by
500 8 m) variability is clearly lost with 10 s averaging, but 10 s averaging preserves most of
501 the variability. Lines in Fig. S2 demark 400 m in altitude, and most of the variability
502 occurs on this larger, model-resolved scale. Fig. S2b shows the 10 s reactivities during
503 that descent and also indicates that much of the variability occurs at 400 m vertical scales.
504 A more quantitative example using all the tropical ATom reactivities is shown in
505 comparisons with probability densities below (Fig. 5).

506 How important is it for the models to represent the extremes of reactivity? While the
507 sorted reactivity curves (Fig. 1, Tables 2 & S8) continue to steepen from the 90th to 97th
508 percentile, the slope does not change that much. Thus we can estimate the 99th+
509 percentile contributes <5% of the total reactivity. Thus, if our model misses the top 1 %
510 of reactive air parcels (e.g., due to the inability to simulate intensely reactive thin
511 pollution layers) then we miss at most 5 % of the total reactivity. This finding is new and
512 encouraging, and it needs to be verified with the ATom-2, 3, and 4 data.

513 The spatial structures and variability of reactivity as sampled by the ATom tropical
514 transects (central Pacific, eastern Pacific and Atlantic) are presented as nine panels in Fig.
515 2. Here, the UCIZ RDS*-2 reactivities are averaged and plotted in 1° latitude by 200 m
516 thick cells, comparable to some global models (e.g., GMI, NCAR, UCI). We separate the
517 eastern Pacific (121° W, research flight (RF) 1) from the Central Pacific (RFs 3, 4 and 5)
518 because we are looking for contiguous latitude-by-pressure structures.

519 In the central Pacific (Fig. 2adg), highly reactive (hot) P-O₃ parcels (> 6 ppb/d) occur in
520 larger, connected air masses at latitudes 20°–22°N and pressure altitudes 2–3 km and in
521 more scattered parcels (> 3 ppb/d) below 5 km down to 20°S. High L-O₃ and L-CH₄
522 coincide with this 20°–22°N air mass and also with some high P-O₃ at lower latitudes.
523 This pattern of overlapping extremes in all three Rs is surprising because the models'
524 mid-Pacific climatologies show a separation between regions of high L-O₃ (lower-middle
525 troposphere) and high P-O₃ (upper troposphere, as seen in P2017's Fig. 3). The obvious
526 explanation is that the models leave most of the lightning-produced NO_x in the upper
527 troposphere. The ATom profiling seems to catch reactive regions in adjacent profiles
528 separate by a few hundred kilometers, scales easily resolvable with 3D models.

529 In the eastern Pacific (Fig. 2beh), the overlap of outbound and return profiles enhances
530 the spatial sampling over the 10 h flight. The region of very large L-O₃ (> 5 ppb/d) is
531 extensive, beginning at 5–6 km at 10°N and broadening to 2–8 km at 28°N. The region
532 of L-CH₄ is similar, but loss at the upper altitudes of this air mass is attenuated because
533 of the temperature dependence of L-CH₄ and possibly because of differing OH:HO₂
534 ratios with altitude. Large P-O₃ (> 3 ppb/day) occurs only in the center of this highly
535 reactive L-O₃/L-CH₄ region, suggesting that NO_x is not as evenly distributed as is HO_x.
536 Highly reactive (hot) P-O₃ parcels (> 4 ppb/day) occur only in the upper troposphere (8–

537 12 km) and only in the sub-tropics. ATom-1 RF1 (29 Jul 2016) occurred during the
538 North American Monsoon when there was easterly flow off Mexico, thus the high
539 reactivity of this large air mass indicates that continental deep convection with lightning
540 NO_x is a source of high reactivity for both O₃ and CH₄.

541 In the Atlantic (Fig. 2cfi) we also see similar air masses through successive profiles,
542 particularly in the northern tropics. The Atlantic P-O₃ shows high-altitude reactivity
543 similar to the eastern Pacific. Likewise, the large values of L-O₃ and L-CH₄ match the
544 eastern Pacific and not central Pacific. Unlike either Pacific transect, the Atlantic L-O₃
545 and L-CH₄ show some high reactivity below 1 km altitude. Overall, the ATom-1
546 profiling clearly identifies extended air masses of high L-O₃ and L-CH₄ extending over
547 2–5 km in altitude and 10° of latitude. The high P-O₃ regions tend to be much more
548 heterogeneous with greatly reduced spatial extent, likely of recent convective origin as
549 for eastern Pacific.

550 Overall, the extensive ATom profiling identifies a heterogeneous mix of chemical
551 composition in the tropical Atlantic and Pacific, with a large range of reactivities. What
552 is important for those trying to model tropospheric chemistry is that the spatial scales of
553 variability seen in Fig. 2 should be within the capability of modern global models.

554 **4.3 Testing model climatologies**

555 The ATom data set provides a unique opportunity to test CTMs and CCMs in a
556 climatological sense. In this section, we compare ATom-1 data and the six models'
557 chemical statistics for mid-August used in P2017. The ATom profiles cannot be easily
558 compared point by point with CCMs, and we use statistical measures of the three
559 reactivities in the three tropical basins: mean profiles in Fig. 3 and PDs in Fig. 5.

560 **4.3.1 Profiles**

561 For P-O₃ profiles (top row, Fig. 3), the agreement between models and measurements is
562 passable except for the 0–2 km region in both Central and Eastern Pacific, where the
563 models fail to predict the observed 2 ppb/d O₃ production. In the Central Pacific at 3–12
564 km, ATom-1 results agree with models, showing ozone production of about 1 ppb/day.
565 In the Eastern Pacific and Atlantic at 3–12 km, ATom-1 results also agree with models,
566 but at a higher ozone production of about 2 ppb/day. This pattern indicates that in the
567 Central Pacific, the NO_x+HO_x combination that produces ozone is suppressed below 2
568 km in all the models. In the upper troposphere, 10–12 km, of the Eastern Pacific and
569 Atlantic, ATom P-O₃ values show a jump to 3 ppb/d, which is only partly reproduced in
570 the models. We take this pattern as evidence for lightning NO_x production and export
571 over the adjacent continents.

572 For L-O₃ (middle row, Fig. 3) in the central Pacific, ATom-1 results match the
573 throughout the 0–12 km range (except GISS). Moving to the eastern Pacific and Atlantic,
574 most models show a mid-level peak above 2 km, while ATom-1 shows even larger peak
575 L-O₃, especially in the Eastern Pacific at 3–6 km where L-O₃ > 4 ppb/d. This mid-
576 tropospheric peak is evident in the curtain plots of Fig. 2 and likely due to easterly mid-
577 tropospheric flow from convection over Mexico at that specific time (29 July 2016).

578 Similarly, the ATom reactivity at 1–3 km in the Atlantic is associated with biomass
579 burning in Africa and was measured in other trace species. Thus, in terms of L-O₃, the
580 ATom–model differences may be due to specific meteorological conditions, and this
581 could be tested with CTMs using 2016 meteorology and wildfires.

582

583 For L-CH₄ (bottom row, Fig. 3), the ATom-model patterns are similar to L-O₃, including
584 the large ATom-only losses (> 1.5 ppb/d over 3–6 km) in the eastern Pacific, but with
585 higher reactivities occurring at slightly lower altitudes because of the large negative
586 temperature dependence of reaction (1). L-O₃ is dominated by O(1D) and HO₂ loss,
587 while L-CH₄ is limited to OH loss. Overall, there is clear evidence that the Atlantic and
588 Pacific have very different chemical mixtures controlling the reactivities and that
589 convection over land (monsoon or biomass burning) creates air masses that are still
590 highly reactive a day or so later.

591

592 **4.3.2 Key species**

593 The deficit in modeled P-O₃ in the central and eastern Pacific at 0–2 km altitude points to
594 a NO_x deficiency in the models, and this becomes obvious in the comparison of the PD
595 histograms for NO_x shown in Fig. 4. Over 0–12 km (first row), ATom has a reduced
596 frequency of parcels with 1–10 ppt and a corresponding increase in parcels with 20–60
597 ppt; this discrepancy is amplified in the lower troposphere, 0–4 km (second row). The
598 obvious source of this oceanic NO_x is lightning since oceanic sources of organonitrates
599 or other nitrate species measured on ATom could not supply this amount. The ATom
600 statistics indicate such a lightning source must be mixed down into the boundary layer.
601 In the eastern Pacific and Atlantic, the full troposphere PD more closely matches the
602 models, including bump in 100–300 ppt NO_x which is probably direct outflow from very
603 deep convection with lightning over the neighboring continents. Overall, the models
604 appear to be missing significant NO_x sources in all three regions below 4 km.

605

606 In Fig. 4, we also look at the histograms for the key HO_x-related species HOOH (third
607 row) and HCHO (fourth row). For these species, the ATom–model agreement is
608 generally good. If anything, the models tend to have too much HOOH. ATom shows
609 systematically large occurrences of low HOOH (50–200 ppt, especially central Pacific)
610 indicating, perhaps, that convective or cloud scavenging of HOOH is more effective than
611 is modeled. HCHO shows reasonable agreement in the Atlantic, but in both central and
612 eastern Pacific, the modeled low end (< 40 ppt) is simply not seen in the ATom data.
613 Also, the models are missing a strong HCHO peak at 300 ppt in the eastern Pacific,
614 probably convection-related specific to that time period. Thus, in terms of these HO_x
615 precursors, the model climatologies appear to be at least as reactive as the ATom data.

616 While the ATom-1 data in Fig. 4 are limited to single transects, the model NO_x
617 discrepancies apply across the three tropical regions, and the simple chemical statistics
618 for these flights alone are probably enough to identify measurement-model discrepancies.
619 For the HO_x-related species, the models match the first-order statistics from ATom. In
620 terms of using ATom statistics as a model metric, it is encouraging that where some
621 individual models tend to deviate from their peers, they also deviate from the ATom-1
622 PDs.

623 4.3.3 Probability densities

624 Mean profiles do not reflect the heterogeneity seen in Fig. 2, and so we also examine the
625 PDs of the tropical reactivities (Fig. 5). The model PDs (colored lines connecting open
626 circles at the center of each bin) are calculated from the 1 d statistics for mid-August
627 (P2017) using the model blocks shown in Fig. S1. The model grid cells are weighted by
628 air mass and cosine(latitude) and limited to pressures greater than 200 hPa. The ATom
629 PDs (black lines connecting black open circles) are calculated from the 10 s data
630 weighted by (but not averaged over) the number of points in each 10° latitude by 200 hPa
631 pressure bin, and then also by cosine (latitude) to compare with the models. In addition,
632 a PD was calculated from the 1° by 200 m average grid-cell values in Fig. 2 (black Xs),
633 and this is also cosine(latitude)-weighted. To check if the high reactivities in the eastern
634 Pacific affected the whole Pacific PD, a separate PD using only central Pacific 10 s data
635 was calculated (gray lines connecting gray open circles). The mean reactivities (ppb/d)
636 from the models and ATom are given in the legend; note that the model values are based
637 on the August climatologies (P2017) and not the MDS-0 values in the table. The 'ATom'
638 legend values are the same as in Table 2. The PD binning is shown by the open circles,
639 and occurrences of off-scale reactivities are included in the last point.

640
641 For the Pacific (eastern + central, left columns, Fig. 5), the modeled PD climatologies are
642 similar for each of the reactivities (except GISS), and there is fairly good agreement with
643 the ATom-1 PDs. For the Atlantic (right columns, Fig. 5), the models show a larger
644 spread presumably due to the differing influence of pollution from neighboring
645 continents. The ATom-1 Atlantic PDs also show slightly larger disagreement with the
646 models (e.g., the maximum in P-O3 at 1–2 ppb/d and minimum in L-O3 at 2–3 ppb/d)
647 and the notably higher frequency of hot spots with L-O3 > 5 ppb/d. The influence of the
648 extreme eastern Pacific reactivities are seen in the statistics generated from the central
649 Pacific values only (CPac, gray circles), e.g., the mean value for L-O3 drops from 1.42 to
650 1.17 ppb/d.

651
652 The ability to test a model's reactivity statistics with the ATom 10 s data is not obvious,
653 but the PDs based on 1° latitude by 200 m altitude cells (the black Xs) are remarkably
654 close to the PDs based on 2 km (horizontal) by 80 m (vertical) 10 s parcels. With the
655 coarser resolution, we see a slight shift of points from the ends of the PD to the middle as
656 expected, but we find once again, that the loss in high-frequency, below-model grid-cell
657 resolution is not great. Both ATom-derived PDs more closely resemble each other than
658 any model PD. Thus, current global chemistry models with resolutions of about 100 km
659 by 400 m should be able to capture much of the wide range of chemical heterogeneity in
660 the atmosphere, which for the oceanic transects is, we believe, adequately resolved by the
661 10 s ATom measurements. Perhaps more surprising, given the different mean profiles in
662 Fig. 3, is that the five model PDs in Fig. 5 look very much alike.

663

664 5 Discussion and path forward

665

666 5.1 Major findings

667

668 This paper opens a door for what the community can do with the ATom measurements
669 and the derived products. ATom's mix of key species allows us to calculate the reactivity
670 of the air parcels and hopefully may become standard for tropospheric chemistry
671 campaigns. We find that the reactivity of the troposphere with respect to O₃ and CH₄ is
672 dominated by a fraction of the air parcels but not by so small and infrequent a fraction as
673 to challenge the ability of current CTMs to simulate these observations and thus be used
674 to study the oxidation budgets. In comparing ATom results with modeled climatologies,
675 we find a systematic ATom-model difference: models show a large relative drop in O₃
676 production below 2 km over the tropical oceans but ATom shows an increase (C.Pac.), no
677 change (E.Pac.) or a much lesser drop (Atl.). We traced this result to the lack of NO_x at
678 20–60 ppt levels in the models below 4 km and believe it provides a clear challenge in
679 modeling ozone.

680 Building our chemical statistics (PDs) from the ATom 10 s air parcels on a scale of 2 km
681 by 80 m, we can identify the fundamental scales of spatial heterogeneity in tropospheric
682 chemistry. Although heterogeneity occurs at the finest scales (such as seen in some 1 s
683 observations) the majority of variability in terms of the O₃ and CH₄ budgets occurs across
684 scales larger than neighboring 2 km parcels. The PDs measured in ATom can be largely
685 captured by a global models' 100 km by 200 m grid cells in the lower troposphere. This
686 surprising result is evident by comparing the ATom 1D PDs – both species and
687 reactivities – with those from the models' climatologies (Fig. 5). These comparisons
688 show that the modeled PDs are consistent with the innate chemical heterogeneity of the
689 troposphere as measured by the 10 s parcels in ATom. A related conclusion for biomass
690 burning smoke particles is found by Schill et al. (2020), where most of the smoke appears
691 in the background rather than in pollution plumes, and therefore much of the variability
692 occurs on synoptic scales resolved by global models (see their Fig. 1 compared with Fig.
693 2 here).

694 **5.2 Opportunities and lessons learned**

695 As a quick look at the opportunities provided by the ATom data, we present an example
696 based on the Wolfe et al (2019) study, which used the F0AM model and semi-analytical
697 arguments to show that troposphere HCHO columns (measurable by satellite and ATom)
698 are related to OH columns (measured by ATom) and thus to CH₄ loss. Fig. 6 extends the
699 Wolfe et al study using the individual air parcels and plotting L-CH₄ (ppb/d) versus
700 HCHO (ppt) for the three tropical regions where most of the CH₄ loss occurs. The
701 relationship is linear but with a lot of scatter and has slopes ranging from 3.5 to 4.4 per
702 day over the three tropical regions; but for the largest reactivities (0–4 km, 1–3 ppb/d), L-
703 CH₄ is not so well correlated with HCHO.

704

705 As is usual with new model intercomparison projects, we have an opportunity to identify
706 model 'features' and identify errors. In the UCI model, an error in the lumped alkane
707 formulation (averaging alkanes C₃H₈ and higher) did not show up in P2018, where UCI
708 supplied all the species, but when the ATom data were used, the UCI model became an
709 outlier. Once found, this problem was readily fixed (hence the current UCIZ model
710 version). Inclusion of the F0AM model with its extensive hydrocarbon oxidation
711 mechanism provided an interesting contrast with the simpler chemistry in the global

712 CCM/CTMs. For a better comparison of the chemical mechanisms, we should have
713 F0AM use 5 d of photolysis fields from one of the CTMs. The anomalous GISS results
714 have been examined by a co-author, but no clear causes have been identified as of this
715 publication. The problem goes beyond just the implementation of the RDS protocol, as it
716 shows up in the model climatology (Fig. 4 & 5, also in P2017).

717 Decadal-scale shifts in the budgets of O₃ and CH₄ are likely to be evident through the
718 statistical patterns of the key species, rather than simply via average profiles. The
719 underlying design of ATom was to collect enough data to develop such a multivariate
720 chemical climatology. As a quick look across the four deployments, we show the joint
721 2D PDs on a logarithmic scale as in P2017 for HOOH versus NO_x in Fig. 7. The patterns
722 for the tropical central Pacific are quite similar for the four seasons of ATom
723 deployments, and the fitted ellipses are almost identical for ATom 2, 3 and 4. Thus, for
724 these species in the central Pacific, we believe that ATom provides a benchmark of the
725 2016-2018 chemical state, one that can be revisited with an aircraft mission in a decade to
726 detect changes in not only chemical composition but also reactivity.

727 ATom identifies which ‘highly reactive’ spatial or chemical environments could be
728 targeted in future campaigns for process studies or to provide a better link between
729 satellite observations and photochemical reactivity (e.g., E. Pacific mid-troposphere in
730 August, Fig. 2). The many corollary species measured by ATom (not directly involved in
731 CH₄ and O₃ chemistry) can provide clues to the origin or chemical processing of these
732 environments. We hope to engage a wider modeling community beyond the ATom
733 science team, as in H2018, in the calculation of photochemical processes, budgets, and
734 feedbacks based on all four ATom deployments.

735

736 *Data Availability.* The MDS-2b and RDS*-2b data for ATom 1, 2, 3 and 4 are presented
737 here as core ATom deliverables, and are posted temporarily on the NASA ESPO ATom
738 website (<https://espo.nasa.gov/atom/content/ATom>) and permanently on DRYAD|UCI
739 (<https://doi.org/10.7280/D1B12H>). This publication marks the public release of the
740 reactivity calculations for ATom 2, 3 and 4, but we have not yet analyzed these data, and
741 thus users should be aware and report any anomalous features to the lead authors via
742 haog2@uci.edu and mprather@uci.edu. Details of the ATom mission and data sets are
743 found on the NASA mission website (<https://espo.nasa.gov/atom/content/ATom>) and at
744 the final archive at Oak Ridge National Laboratory (ORNL;
745 https://daac.ornl.gov/ATOM/guides/ATom_merge.html). The MATLAB scripts and data
746 sets used in the analysis here are posted on Dryad (<https://doi.org/10.7280/D1Q699>).

747 *Supplement.* The supplement related to this article is available online at:
748 <https://doi.org/10.5194/acp-21-13729-2021-supplement>.

749 *Author Contributions.* HG, CMF, SCW and MJP designed the research and performed
750 the data analysis. SAS, SDS, LE, FL, JL, AMF, GC, LTM and GW contributed original
751 atmospheric chemistry model results. GW, MK, JC, GD, JD, BCD, RC, KM, JP, TBR,
752 CT, TFH, DB, NJB, ECA, RSH, JE, EH and FM contributed original atmospheric
753 observations. HG, CMF and MJP wrote the paper.

754 *Competing interests.* The contact author has declared that neither they nor their co-
755 authors have any competing interests

756 *Acknowledgments.* The authors are indebted to the entire ATom Science Team including
757 the managers, pilots and crew, who made this mission possible. Many other scientists not
758 on the author list enabled the measurements and model results used here. The authors
759 thank Ms. Xin Zhu for maintaining and updating the UCI Chemistry Transport Model
760 used here.

761

762 *Financial support.* The Atmospheric Tomography Mission (ATom) was supported by the
763 National Aeronautics and Space Administration's Earth System Science Pathfinder
764 Venture-Class Science Investigations: Earth Venture Suborbital-2. Primary funding of the
765 preparation of this paper at UC Irvine was through NASA (grant nos. NNX15AG57A and
766 80NSSC21K1454).

767

768 *Review statement.* This paper was edited by Neil Harris and reviewed by two anonymous
769 referees.

770

771 **References**

- 772 Burkholder, J. B., Sander, S. P., Abbatt, J. P. D., Barker, J. R., Huie, R. E., Kolb, C. E.,
773 Kurylo, M. J., Orkin, V. L., Wilmouth, D. M., and Wine, P. H.: Chemical kinetics and
774 photochemical data for use in atmospheric studies: evaluation number 18, Pasadena, CA,
775 Jet Propulsion Laboratory, National Aeronautics and Space Administration, available at:
776 <http://hdl.handle.net/2014/45510> (last access: 13 September 2021), 2015.
- 777 Charlton-Perez, C. L., Evans, M. J., Marsham, J. H., and Esler, J. G.: The impact of
778 resolution on ship plume simulations with NO_x chemistry, *Atmos. Chem. Phys.*, 9, 7505–
779 7518, <https://doi.org/10.5194/acp-9-7505-2009>, 2009.
- 780 Douglass, A. R., Prather, M. J., Hall, T. M., Strahan, S. E., Rasch, P. J., Sparling, L. C.,
781 Coy, L., and Rodriguez, J. M.: Choosing meteorological input for the global modeling
782 initiative assessment of high-speed aircraft, *J. Geophys. Res.-Atmos.*, 104, 27545–27564,
783 <https://doi.org/10.1029/1999JD900827>, 1999.
- 784 Eastham, S. D. and Jacob, D. J.: Limits on the ability of global Eulerian models to resolve
785 intercontinental transport of chemical plumes, *Atmos. Chem. Phys.*, 17, 2543–2553,
786 <https://doi.org/10.5194/acp-17-2543-2017>, 2017.
- 787 Griffiths, P. T., Murray, L. T., Zeng, G., Shin, Y. M., Abraham, N. L., Archibald, A. T.,
788 Deushi, M., Emmons, L. K., Galbally, I. E., Hassler, B., Horowitz, L. W., Keeble, J., Liu,
789 J., Moeini, O., Naik, V., O'Connor, F. M., Oshima, N., Tarasick, D., Tilmes, S., Turnock,
790 S. T., Wild, O., Young, P. J., and Zanis, P.: Tropospheric ozone in CMIP6 simulations,
791 *Atmos. Chem. Phys.*, 21, 4187–4218, <https://doi.org/10.5194/acp-21-4187-2021>, 2021.
- 792 Guo, H.: Heterogeneity and chemical reactivity of the remote Troposphere defined by
793 aircraft measurements, Dryad [data set], <https://doi.org/10.7280/D1Q699>, 2021.
- 794 Hall, S. R., Ullmann, K., Prather, M. J., Flynn, C. M., Murray, L. T., Fiore, A. M.,
795 Correa, G., Strode, S. A., Steenrod, S. D., Lamarque, J.-F., Guth, J., Josse, B., Flemming,
796 J., Huijnen, V., Abraham, N. L., and Archibald, A. T.: Cloud impacts on photochemistry:
797 building a climatology of photolysis rates from the Atmospheric Tomography mission,
798 *Atmos. Chem. Phys.*, 18, 16809–16828, <https://doi.org/10.5194/acp-18-16809-2018>,
799 2018.
- 800 Heald, C. L., Coe, H., Jimenez, J. L., Weber, R. J., Bahreini, R., Middlebrook, A. M.,
801 Russell, L. M., Jolleys, M., Fu, T.-M., Allan, J. D., Bower, K. N., Capes, G., Crosier, J.,
802 Morgan, W. T., Robinson, N. H., Williams, P. I., Cubison, M. J., DeCarlo, P. F., and
803 Dunlea, E. J.: Exploring the vertical profile of atmospheric organic aerosol: comparing 17
804 aircraft field campaigns with a global model, *Atmos. Chem. Phys.*, 11, 12673–12696,
805 <https://doi.org/10.5194/acp-11-12673-2011>, 2011.
- 806 Myhre, G., Shindell, D., and Pongratz, J.: Anthropogenic and Natural Radiative Forcing,
807 in *Climate Change 2013: The Physical Science Basis*, IPCC WGI Contribution to the

808 Fifth Assessment Report, Cambridge University Press, 659–740,
809 <https://doi.org/10.1017/CBO9781107415324.018>, 2014.

810 Naik, V., Voulgarakis, A., Fiore, A. M., Horowitz, L. W., Lamarque, J.-F., Lin, M.,
811 Prather, M. J., Young, P. J., Bergmann, D., Cameron-Smith, P. J., Cionni, I., Collins, W.
812 J., Dalsøren, S. B., Doherty, R., Eyring, V., Faluvegi, G., Folberth, G. A., Josse, B., Lee,
813 Y. H., MacKenzie, I. A., Nagashima, T., van Noije, T. P. C., Plummer, D. A., Righi, M.,
814 Rumbold, S. T., Skeie, R., Shindell, D. T., Stevenson, D. S., Strode, S., Sudo, K., Szopa,
815 S., and Zeng, G.: Preindustrial to present-day changes in tropospheric hydroxyl radical
816 and methane lifetime from the Atmospheric Chemistry and Climate Model
817 Intercomparison Project (ACCMIP), *Atmos. Chem. Phys.*, 13, 5277–5298,
818 <https://doi.org/10.5194/acp-13-5277-2013>, 2013.

819 Prather, M. J., Ehhalt, D., Dentener, F., Derwent, R., Dlugokencky, E. J., Holland, E.,
820 Isaksen, I., Katima, J., Kirchhoff, V., Matson, P., and Midgley, P.: Chapter 4 –
821 Atmospheric Chemistry and Greenhouse Gases, *Climate Change 2001: The Scientific*
822 *Basis, Third Assessment Report of the Intergovernmental Panel on Climate Change*, 239–
823 287, 2001.

824 Prather, M. J., Zhu, X., Flynn, C. M., Strode, S. A., Rodriguez, J. M., Steenrod, S. D.,
825 Liu, J., Lamarque, J.-F., Fiore, A. M., Horowitz, L. W., Mao, J., Murray, L. T., Shindell,
826 D. T., and Wofsy, S. C.: Global atmospheric chemistry – which air matters, *Atmos.*
827 *Chem. Phys.*, 17, 9081–9102, <https://doi.org/10.5194/acp-17-9081-2017>, 2017.

828 Prather, M. J., Flynn, C. M., Zhu, X., Steenrod, S. D., Strode, S. A., Fiore, A. M., Correa,
829 G., Murray, L. T., and Lamarque, J.-F.: How well can global chemistry models calculate
830 the reactivity of short-lived greenhouse gases in the remote troposphere, knowing the
831 chemical composition, *Atmos. Meas. Tech.*, 11, 2653–2668, [https://doi.org/10.5194/amt-](https://doi.org/10.5194/amt-11-2653-2018)
832 [11-2653-2018](https://doi.org/10.5194/amt-11-2653-2018), 2018.

833 Rastigejev, Y., Park, R., Brenner, M. P., and Jacob, D. J.: Resolving intercontinental
834 pollution plumes in global models of atmospheric transport, *J. Geophys. Res.-Atmos.*,
835 115, D012568, <https://doi.org/10.1029/2009JD012568>, 2010.

836 Schill, G. P., Froyd, K. D., Bian, H., Kupc, A., Williamson, C., Brock, C. A., Ray, E.,
837 Hornbrook, R. S., Hills, A. J., Apel, E. C., and Chin, M.: Widespread biomass burning
838 smoke throughout the remote troposphere, *Nat. Geosci.*, 13, 422–427,
839 <https://doi.org/10.1038/s41561-020-0586-1>, 2020.

840 Science team of the NASA Atmospheric Tomography Mission: ATom [data set],
841 available at: <https://espo.nasa.gov/atom/content/ATom>, last access: 13 September 2021.

842 Stevenson, D. S., Dentener, F. J., Schultz, M. G., Ellingsen, K., Van Noije, T. P. C.,
843 Wild, O., Zeng, G., Amann, M., Atherton, C. S., Bell, N., and Bergmann, D. J.:
844 Multimodel ensemble simulations of present-day and near-future tropospheric ozone, *J.*
845 *Geophys. Res.-Atmos.*, 111, D006338, <https://doi.org/10.1029/2005JD006338>, 2006.

846 Stevenson, D. S., Young, P. J., Naik, V., Lamarque, J.-F., Shindell, D. T., Voulgarakis,
847 A., Skeie, R. B., Dalsoren, S. B., Myhre, G., Berntsen, T. K., Folberth, G. A., Rumbold,
848 S. T., Collins, W. J., MacKenzie, I. A., Doherty, R. M., Zeng, G., van Noije, T. P. C.,
849 Strunk, A., Bergmann, D., Cameron-Smith, P., Plummer, D. A., Strode, S. A., Horowitz,
850 L., Lee, Y. H., Szopa, S., Sudo, K., Nagashima, T., Josse, B., Cionni, I., Righi, M.,
851 Eyring, V., Conley, A., Bowman, K. W., Wild, O., and Archibald, A.: Tropospheric
852 ozone changes, radiative forcing and attribution to emissions in the Atmospheric
853 Chemistry and Climate Model Intercomparison Project (ACCMIP), *Atmos. Chem. Phys.*,
854 13, 3063–3085, <https://doi.org/10.5194/acp-13-3063-2013>, 2013.

855 Stevenson, D. S., Zhao, A., Naik, V., O'Connor, F. M., Tilmes, S., Zeng, G., Murray, L.
856 T., Collins, W. J., Griffiths, P. T., Shim, S., Horowitz, L. W., Sentman, L. T., and
857 Emmons, L.: Trends in global tropospheric hydroxyl radical and methane lifetime since
858 1850 from AerChemMIP, *Atmos. Chem. Phys.*, 20, 12905–12920,
859 <https://doi.org/10.5194/acp-20-12905-2020>, 2020.

860 Stocker, T. F., Qin, D., Plattner, G. K., Tignor, M., Allen, S. K., Boschung, J., Nauels, A.,
861 Xia, Y., Bex, V., and Midgley, P. M.: Contribution of working group I to the fifth
862 assessment report of the intergovernmental panel on climate change. Cambridge
863 University Press, 33–115, 2013.

864 Tie, X., Brasseur, G., and Ying, Z.: Impact of model resolution on chemical ozone
865 formation in Mexico City: application of the WRF-Chem model, *Atmos. Chem. Phys.*,
866 10, 8983–8995, <https://doi.org/10.5194/acp-10-8983-2010>, 2010.

867 Voulgarakis, A., Naik, V., Lamarque, J.-F., Shindell, D. T., Young, P. J., Prather, M. J.,
868 Wild, O., Field, R. D., Bergmann, D., Cameron-Smith, P., Cionni, I., Collins, W. J.,
869 Dalsøren, S. B., Doherty, R. M., Eyring, V., Faluvegi, G., Folberth, G. A., Horowitz, L.
870 W., Josse, B., MacKenzie, I. A., Nagashima, T., Plummer, D. A., Righi, M., Rumbold, S.
871 T., Stevenson, D. S., Strode, S. A., Sudo, K., Szopa, S., and Zeng, G.: Analysis of present
872 day and future OH and methane lifetime in the ACCMIP simulations, *Atmos. Chem.*
873 *Phys.*, 13, 2563–2587, <https://doi.org/10.5194/acp-13-2563-2013>, 2013.

874 Wofsy, S. C.: HIAPER Pole-to-Pole Observations (HIPPO): fine-grained, global-scale
875 measurements of climatically important atmospheric gases and aerosols, *Philos. T. R.*
876 *Soc. A*, 369, 2073–2086, <https://doi.org/10.1098/rsta.2010.0313>, 2011.

877 Wofsy, S. C., Afshar, S., Allen, H. M., Apel, E. C., Asher, E. C., Barletta, B., Bent, J.,
878 Bian, H., Biggs, B. C., Blake, D. R., Blake, N., Bourgeois, I., Brock, C. A., Brune, W. H.,
879 Budney, J. W., Bui, T. P., Butler, A., Campuzano-Jost, P., Chang, C.S., Chin, M.,
880 Commane, R., Correa, G., Crouse, J. D., Cullis, P. D., Daube, B.C., Day, D. A., Dean-
881 Day, J. M., Dibb, J. E., DiGangi, J. P., Diskin, G. S., Dollner, M., Elkins, J. W., Erdesz,
882 F., Fiore, A. M., Flynn, C. M., Froyd, K. D., Gesler, D. W., Hall, S. R., Hanisco, T. F.,
883 Hannun, R. A., Hills, A. J., Hints, E. J., Hoffman, A., Hornbrook, R. S., Huey, L. G.,
884 Hughes, S., Jimenez, J. L., Johnson, B. J., Katich, J. M., Keeling, R. F., Kim, M. J.,
885 Kupc, A., Lait, L. R., Lamarque, J.-F., Liu, J., McKain, K., Mclaughlin, R. J., Meinardi,

886 S., Miller, D. O., Montzka, S. A., Moore, F. L., Morgan, E. J., Murphy, D. M., Murray, L.
887 T., Nault, B. A., Neuman, J. A., Newman, P. A., Nicely, J. M., Pan, X., Paplawsky, W.,
888 Peischl, J., Prather, M. J., Price, D. J., Ray, E. A., Reeves, J. M., Richardson, M., Rollins,
889 A. W., Rosenlof, K. H., Ryerson, T. B., Scheuer, E., Schill, G. P., Schroder, J. C.,
890 Schwarz, J. P., St.Clair, J. M., Steenrod, S. D., Stephens, B. B., Strode, S. A., Sweeney,
891 C., Tanner, D., Teng, A. P., Thames, A. B., Thompson, C. R., Ullmann, K., Veres, P. R.,
892 Vieznor, N., Wagner, N. L., Watt, A., Weber, R., Weinzierl, B., Wennberg, P. O.,
893 Williamson, C. J., Wilson, J. C., Wolfe, G. M., Woods, C. T., and Zeng L. H.: ATom:
894 Merged Atmospheric Chemistry, Trace Gases, and Aerosols, ORNL DAAC [data set],
895 Oak Ridge, Tennessee, USA, <https://doi.org/10.3334/ORNLDAAC/1581>, 2018.

896 Wolfe, G. M., Nicely, J. M., Clair, J. M. S., Hanisco, T. F., Liao, J., Oman, L. D., Brune,
897 W. B., Miller, D., Thames, A., Abad, G. G., and Ryerson, T. B.: Mapping hydroxyl
898 variability throughout the global remote troposphere via synthesis of airborne and
899 satellite formaldehyde observations, *P. Natl. Acad. Sci. USA*, 116, 11171–11180,
900 <https://doi.org/10.1073/pnas.1821661116>, 2019.

901 Young, P. J., Archibald, A. T., Bowman, K. W., Lamarque, J.-F., Naik, V., Stevenson, D.
902 S., Tilmes, S., Voulgarakis, A., Wild, O., Bergmann, D., Cameron-Smith, P., Cionni, I.,
903 Collins, W. J., Dalsøren, S. B., Doherty, R. M., Eyring, V., Faluvegi, G., Horowitz, L.
904 W., Josse, B., Lee, Y. H., MacKenzie, I. A., Nagashima, T., Plummer, D. A., Righi, M.,
905 Rumbold, S. T., Skeie, R. B., Shindell, D. T., Strode, S. A., Sudo, K., Szopa, S., and
906 Zeng, G.: Pre-industrial to end 21st century projections of tropospheric ozone from the
907 Atmospheric Chemistry and Climate Model Intercomparison Project (ACCMIP), *Atmos.*
908 *Chem. Phys.*, 13, 2063–2090, <https://doi.org/10.5194/acp-13-2063-2013>, 2013.

909 Young, P. J., Naik, V., Fiore, A. M., Gaudel, A., Guo, J., Lin, M. Y., Neu, J. L., Parrish,
910 D. D., Rieder, H. E., Schnell, J. L., and Tilmes, S.: Tropospheric Ozone Assessment
911 Report: Assessment of global-scale model performance for global and regional ozone
912 distributions, variability, and trends, *Elementa*, 6, 10,
913 <https://doi.org/10.1525/elementa.265>, 2018.

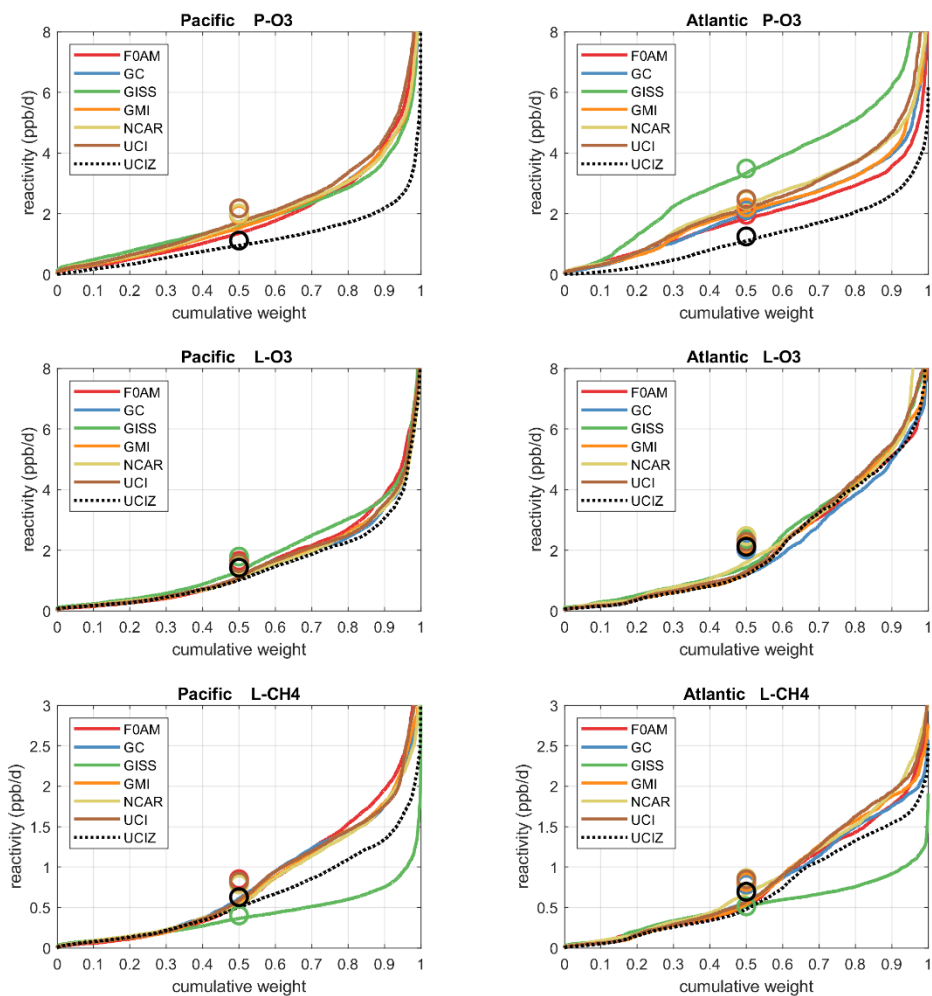
914 Yu, K., Jacob, D. J., Fisher, J. A., Kim, P. S., Marais, E. A., Miller, C. C., Travis, K. R.,
915 Zhu, L., Yantosca, R. M., Sulprizio, M. P., Cohen, R. C., Dibb, J. E., Fried, A.,
916 Mikoviny, T., Ryerson, T. B., Wennberg, P. O., and Wisthaler, A.: Sensitivity to grid
917 resolution in the ability of a chemical transport model to simulate observed oxidant
918 chemistry under high-isoprene conditions, *Atmos. Chem. Phys.*, 16, 4369–4378,
919 <https://doi.org/10.5194/acp-16-4369-2016>, 2016.

920 Zhuang, J., Jacob, D. J., and Eastham, S. D.: The importance of vertical resolution in the
921 free troposphere for modeling intercontinental plumes, *Atmos. Chem. Phys.*, 18, 6039–
922 6055, <https://doi.org/10.5194/acp-18-6039-2018>, 2018.

923

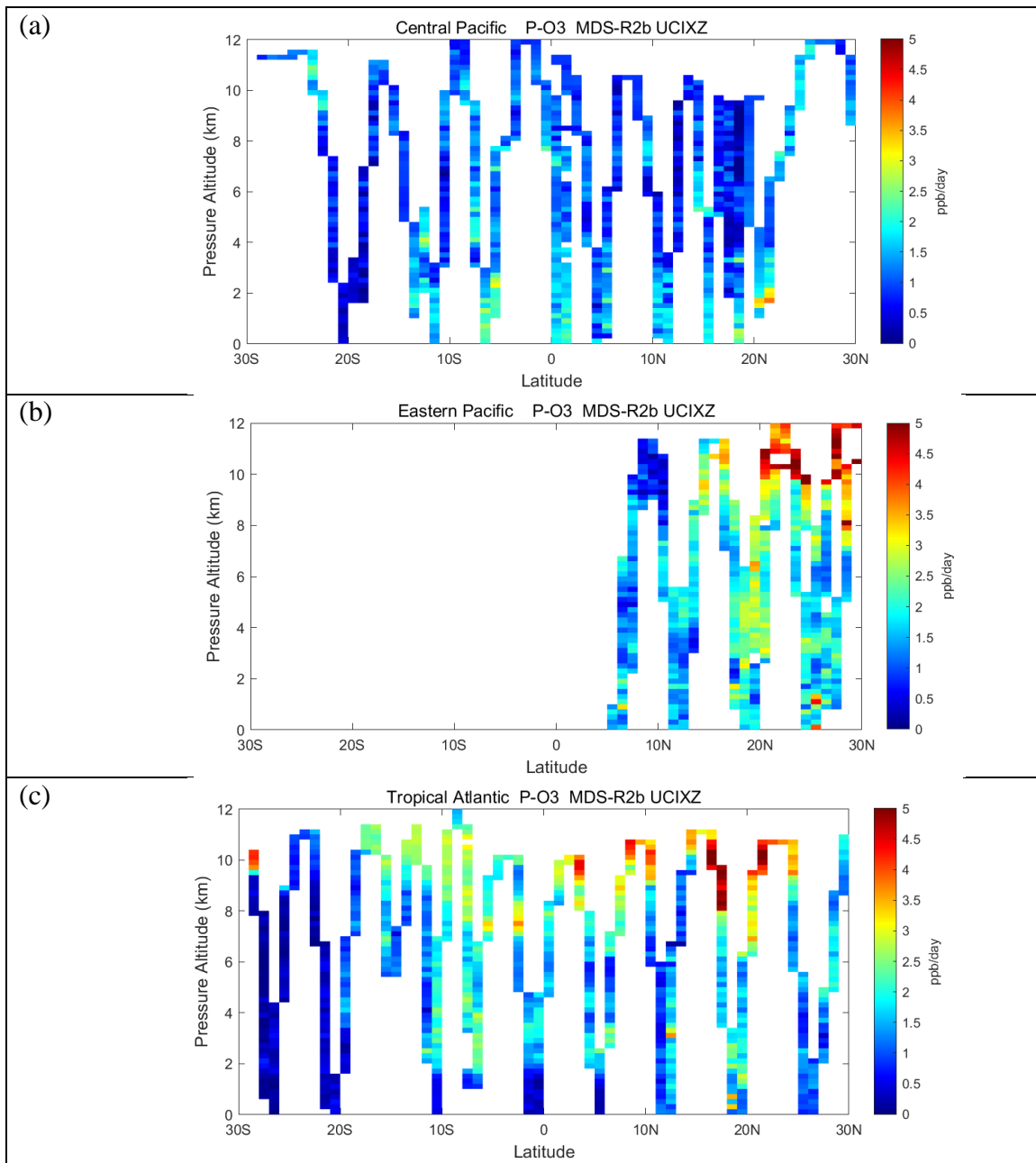
924
925

Figures and Tables

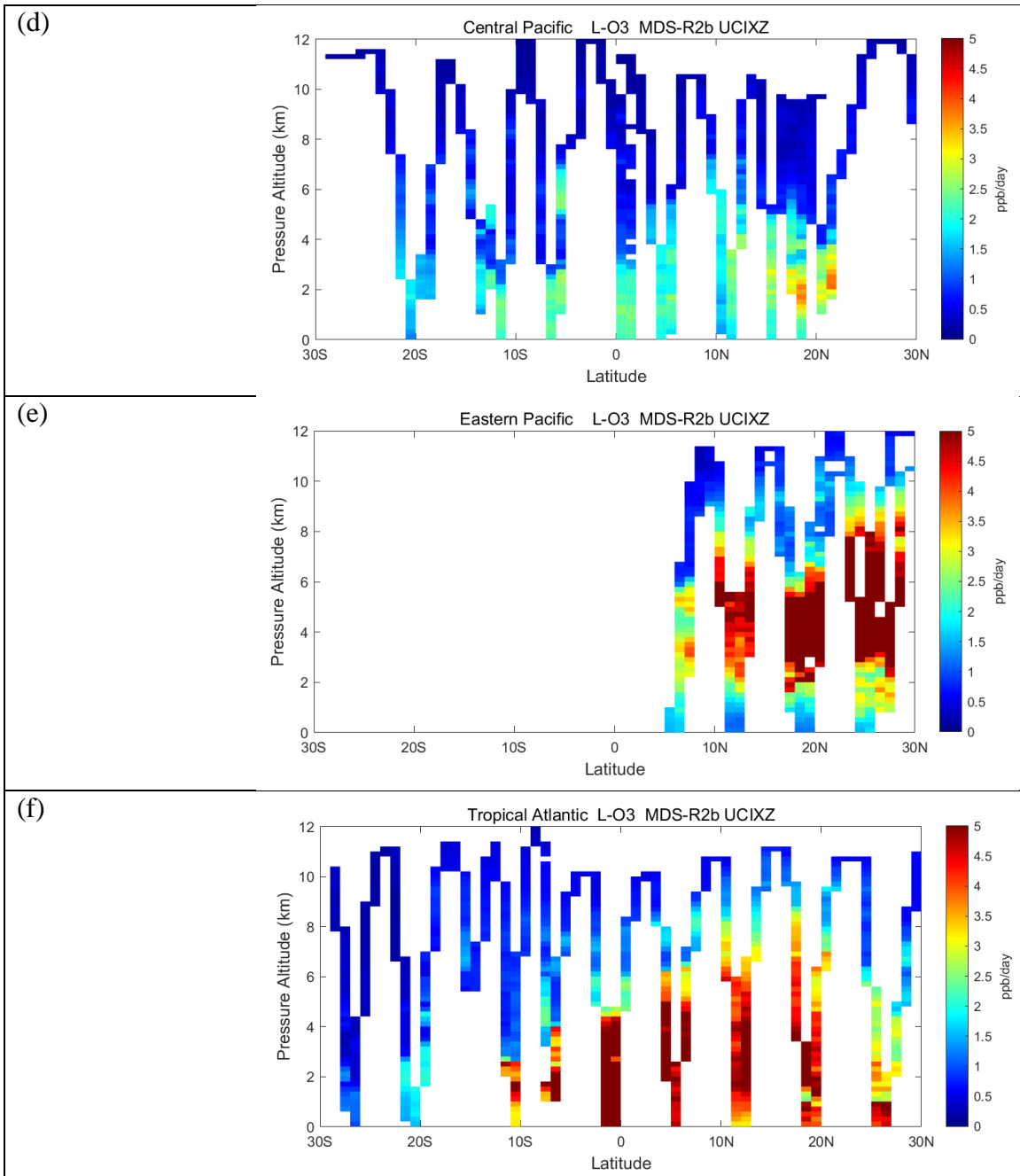


926
927
928
929
930
931
932
933
934
935
936

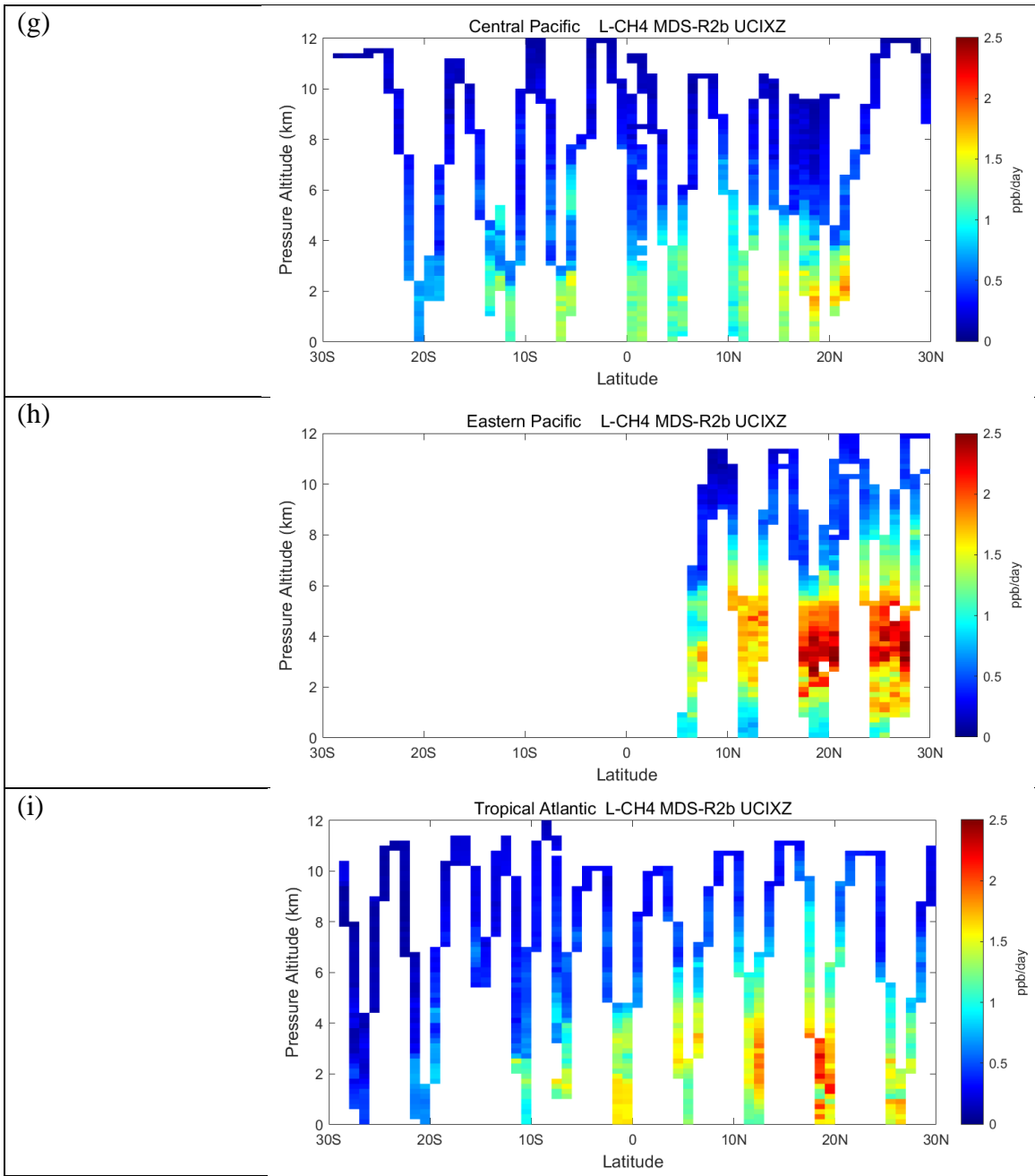
Fig. 1. Sorted reactivities (P-O3, L-O3, L-CH4, ppb/day; three successive rows) for the Pacific and Atlantic domains (53° S–60° N, two columns) of ATom-1. Each parcel is weighted, including cosine(latitude), see text. Results from six models using MDS-0 and the standard RDS protocol are shown with colored lines; the updated UCIZ CTM using MDS-2b with the RDS* protocol (HNO₄ and PAN damping) is shown as a black dashed line. The mean value for each model is shown with an open circle plotted at the 50th percentile. (Flipped about the axes, this is a cumulative probability density function.)



938 **Fig. 2abc.** Curtain plots for P-O3 (0–5 ppb/d; Fig 2abc), L-O3 (0–5 ppb/d; Fig 2def) and L-CH4
 939 (0–2.5 ppb/d; Fig 2ghi) showing the profiling of ATom-1 flights in the central Pacific (RF 3, 4
 940 and 5; Fig 2adg), eastern Pacific (RF 1; Fig2 beh), and Atlantic (RF 7, 8, and 9; Fig2cfi).
 941 Reactivities are calculated with the current UCIZ CTM model using MDS-2b and the RDS*
 942 protocol, see text. The 10 s air parcels are averaged into 1° latitude and 200 m altitude bins.
 943

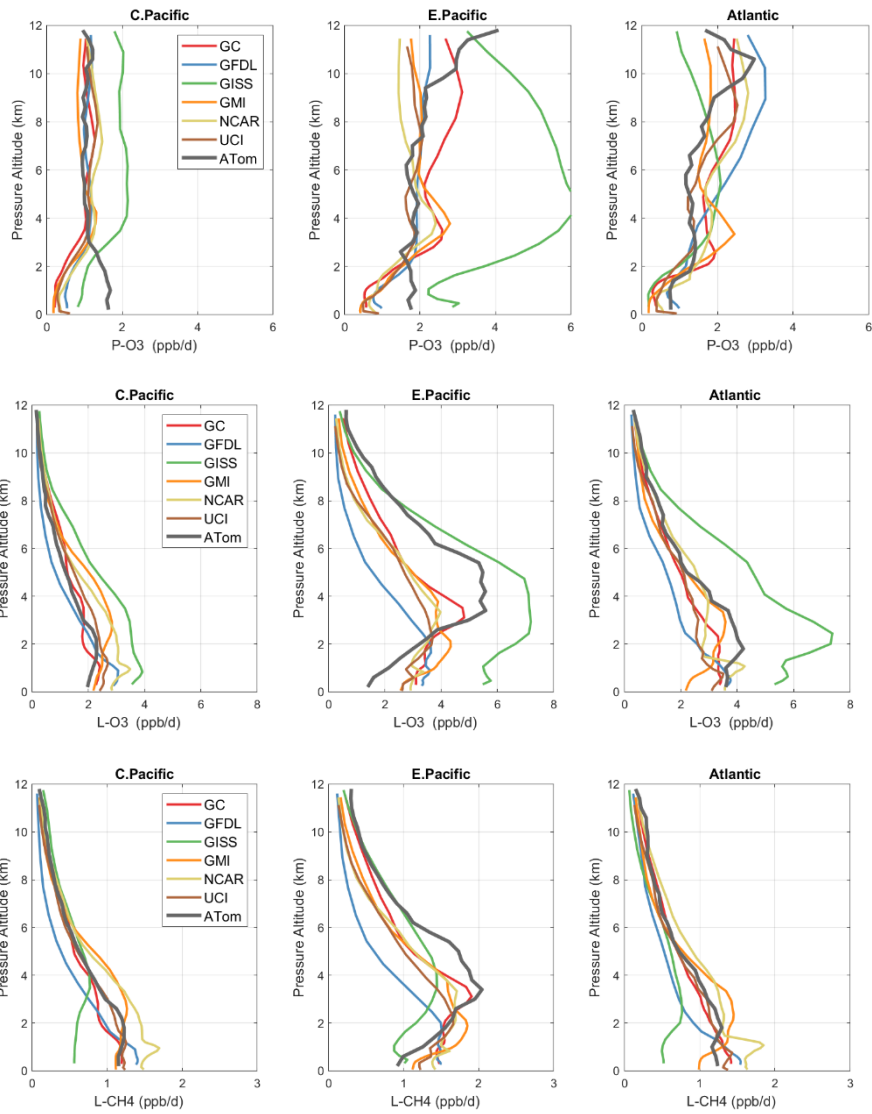


944 **Fig. 2def.**
945
946



947 **Fig. 2ghi.**
948
949

950

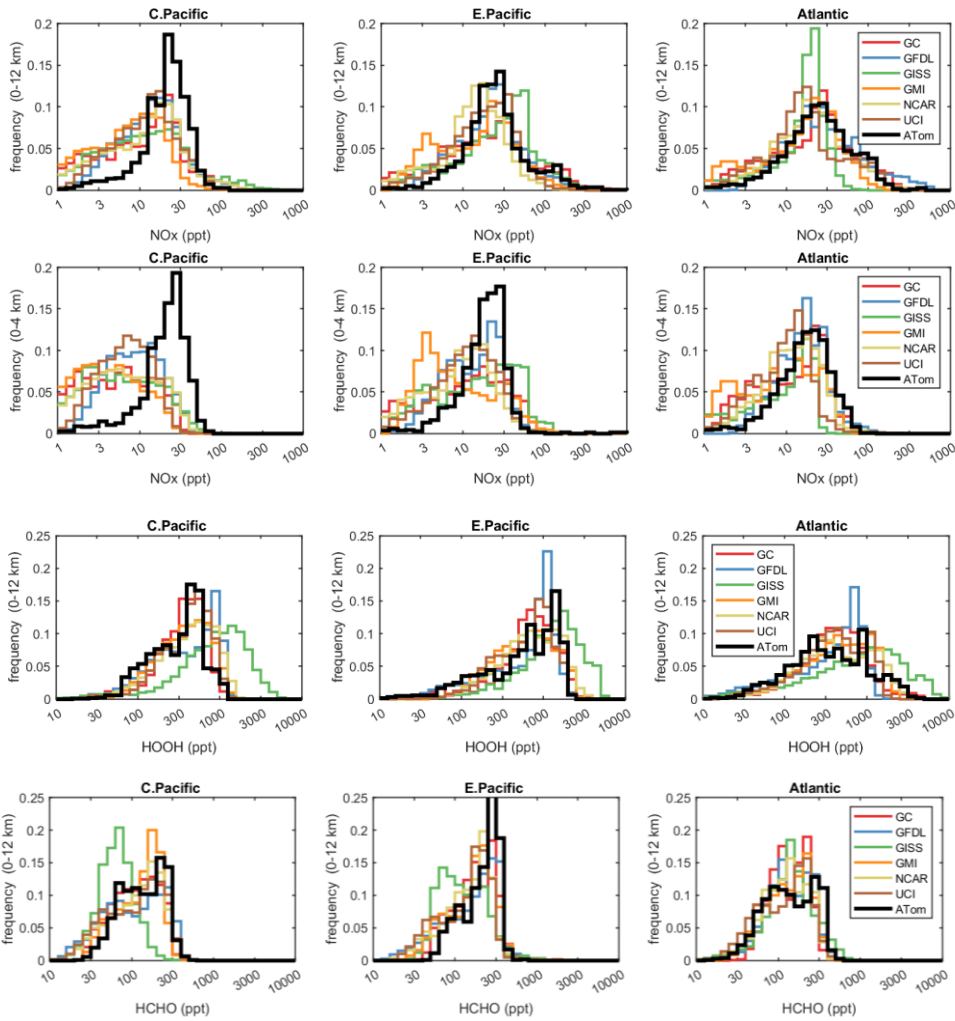


951

952

953 **Fig. 3.** Mean altitude profiles of reactivity (rows: P-O3, L-O3, L-CH4 in ppb/day) in 3 domains
954 (columns: C. Pacific, 30° S–30° N by 180°–210° E; E. Pacific, 0°–30° N by 230°–250° E;
955 Atlantic, 30° S–30° N by 326°–343° E; ranges are the model blocks). Air parcels are
956 cosine(latitude) weighted. ATom-1 (gray) results are from Fig. 2, while model results are taken
957 from the August climatologies in Prather et al. (2017).

958



959

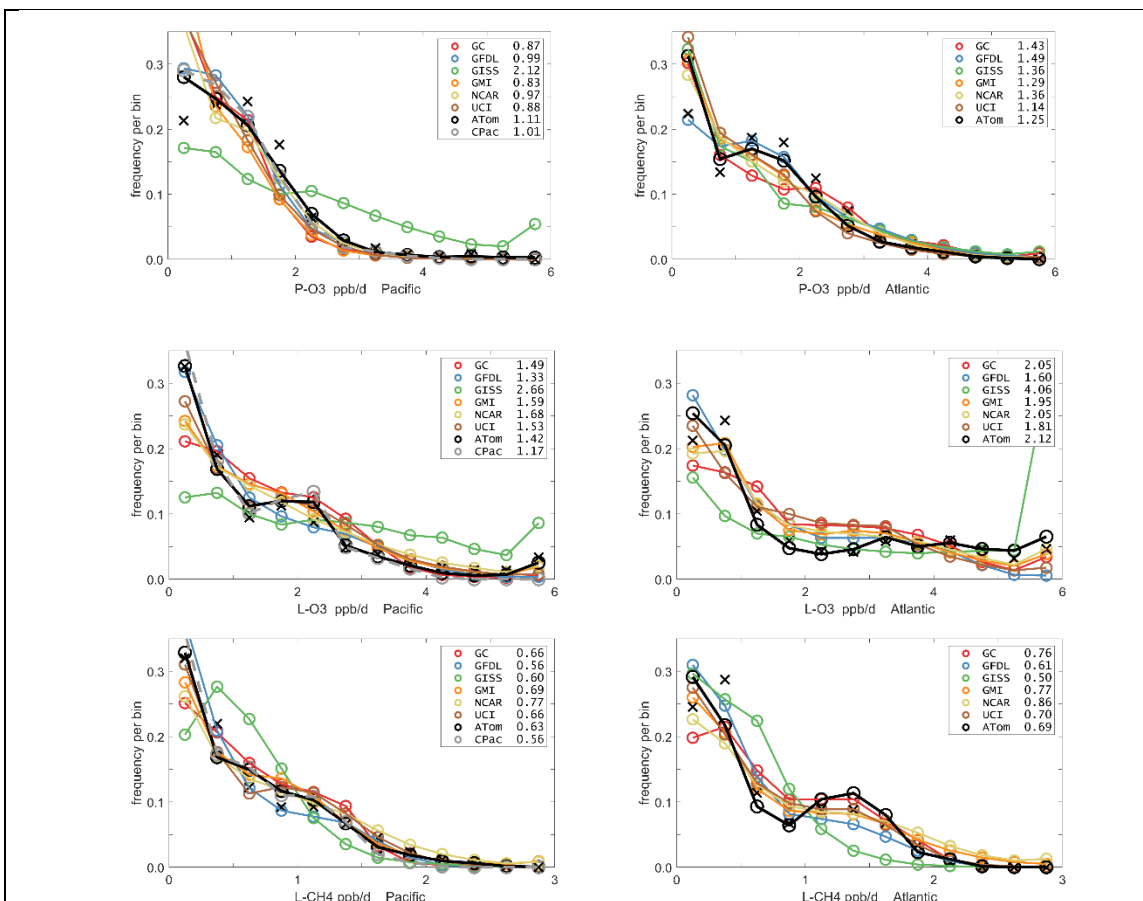
960

961

962 **Fig. 4.** Histograms of probability densities (PDs) of NO_x (0–12 km, row 1), NO_x (0–4 km, row 2),
 963 HOOH (0–12 km, row 3), and HCHO (0–12 km, row 4) for the three tropical regions (central
 964 Pacific, eastern Pacific, Atlantic). The ATom-1 data is plotted on top of the six global chemistry
 965 models' results for a day in mid-August and sampled as described in Fig. 3.

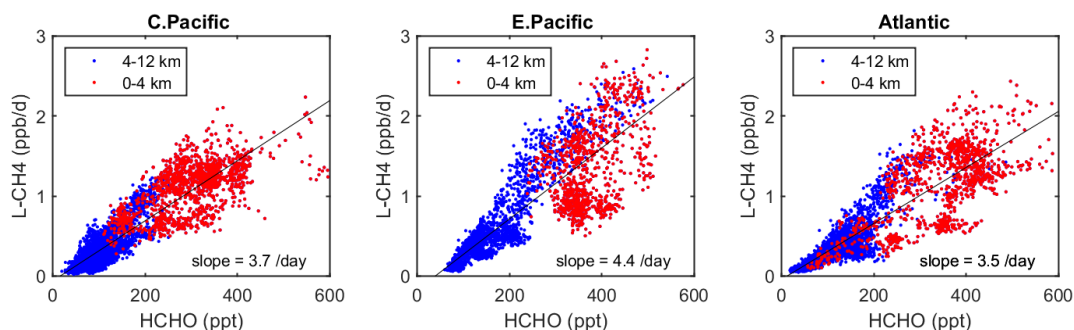
966

967



968
 969
 970
 971
 972
 973
 974
 975
 976
 977
 978
 979

Fig. 5. Probability densities (PD, frequency of occurrence) for the ATom-1 three reactivities (rows: P-O3, L-O3, L-CH4 in ppb/day) and for the Pacific and Atlantic from 53° S to 60° N (columns left and right). Each air parcel is weighted as described in the text for equal frequency in large latitude-pressure bins, and also by cosine(latitude). The ATom statistics are from the UCIZ model, using MDS-2b and revised RDS* protocol (HNO₄ and PAN damping). The Pacific results (solid black) also show the central Pacific alone (dashed gray). The six models' values for a day in mid-August are averaged over longitude for the domains shown in Fig. S1 in the Supplement, and then cosine(latitude) weighted. Mean values (ppb/day) are shown in the legend. The PD derived from the ATom 10 s parcels binned into 1° latitude by 200 m altitude (as shown for the tropics in Fig. 2) is typical of a high-resolution global model, and denoted by black Xs.



980
 981 **Fig. 6.** Scatterplot of L-CH₄ (ppb/d) versus HCHO (ppt) for ATom 1 in the 3 tropical regions
 982 shown in **Fig. 3**. The air parcels are split into lower troposphere (0–4 km pressure altitude, red
 983 dots) where most of the reactivity lies and mid+upper troposphere (4–12 km, blue). A simple
 984 linear fit to all data is shown (thin black line) and the slope is given in units of 1/day.
 985
 986

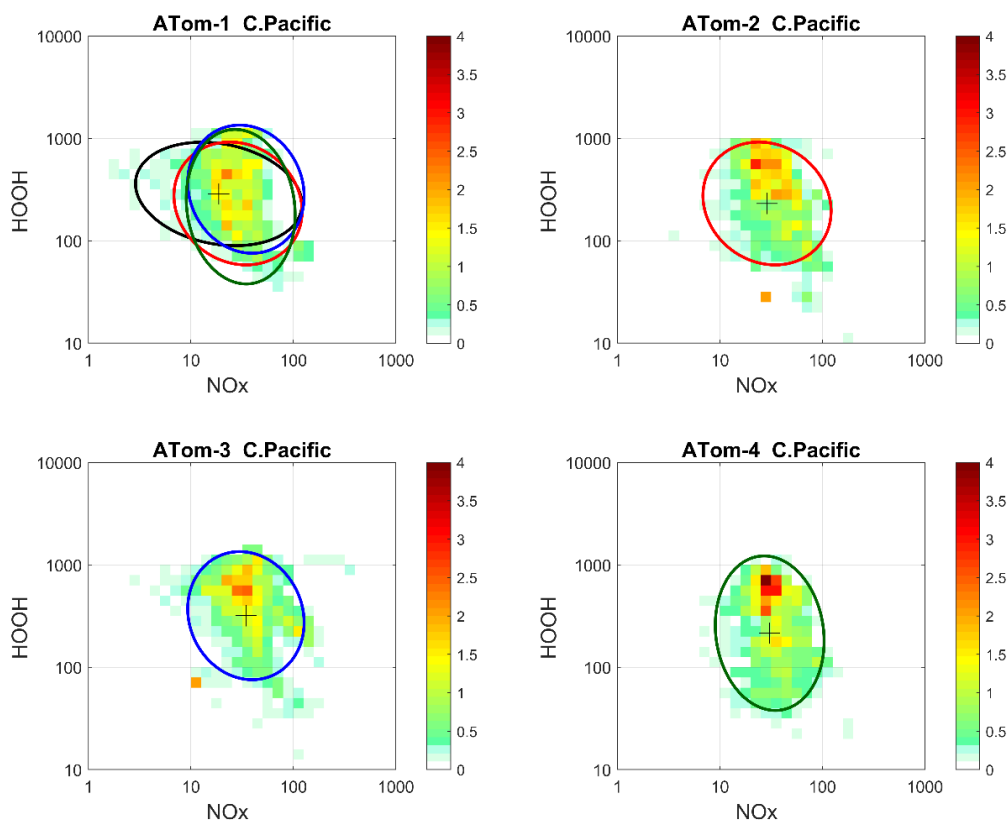


Fig. 7. 2D frequency of occurrence (PDs in log ppt mole fraction) of HOOH vs. NO_x for the tropical Central Pacific for all 4 ATom deployments. The cross marks the mean (in log space), and the ellipse is fitted to the rotated PD having the smallest semi-minor axis. The semi-minor and semi-major axes are 2 standard deviations of PD in that direction. The ellipses from ATom-2 (red), ATom-3 (blue), and ATom-4 (dark green) are also plotted in the ATom-1 quadrant.

987

Used for	ID	Model name	Model type	Meteorology	Model Grid
clim	GFDL	GFDL-AM3	CCM	NCEP (nudged)	C180 x L48
clim, MDS-0	GISS	GISS-E2.1	CCM	Daily SSTs, nudged to MERRA	2° x 2.5° x 40L
clim, MDS-0	GMI	GMI-CTM	CTM	MERRA	1° x 1.25° x 72L
clim, MDS-0	GC	GEOS-Chem	CTM	MERRA-2	2° x 2.5° x 72L
clim, MDS-0	NCAR	CAM4-Chem	CCM	Nudged to MERRA	0.47° x 0.625° x 52L
clim, MDS-0 & 2b	UCI	UCI-CTM	CTM	ECMWF IFS Cy38r1	T159N80 x L60
MDS-0	FOAM	FOAM	box	MDS + scaled ATom Js	N/A

988 The descriptions of models used in the paper. The first column denotes if the model's August
989 climatology is used ('clim') and also the MDS versions used. FOAM used chemical mechanism
990 MCMv331 plus J-HNO₄ plus O¹D)+CH₄. For the global models see P2017, P2017, and H2018.
991

Table 2. Reactivity statistics for the three large domains (global, Pacific, Atlantic).

Value	Region	Models using MDS-0								MDS-2b
		F0AM	GC	GISS	GMI	NCAR	UCI	U15	U97	UCIZ*
P-O3, mean, ppb/d	Global	2.12	2.12	2.57	2.08	2.22	2.38	2.37	2.37	1.23
	Pacific	1.96	2.00	1.99	e1.9 6	2.01	2.17	2.13	2.15	1.11
	Atlantic	1.96	2.12	3.49	2.20	2.44	2.48	2.48	2.49	1.25
L-O3, mean, ppb/d	Global	1.81	1.63	1.93	1.70	1.76	1.76	1.74	1.75	1.61
	Pacific	1.65	1.51	1.79	1.55	1.52	1.58	1.53	1.56	1.42
	Atlantic	2.15	2.02	2.37	2.17	2.47	2.28	2.28	2.30	2.12
L-CH4, mean, ppb/d	Global	0.81	0.76	0.43	0.75	0.73	0.79	0.78	0.78	0.61
	Pacific	0.85	0.82	0.40	0.80	0.79	0.82	0.80	0.81	0.63
	Atlantic	0.80	0.78	0.51	0.81	0.86	0.85	0.85	0.85	0.69
P-O3, %sum R in top 10%	Global	35%	32%	31%	32%	30%	34%	34%	34%	33%
	Pacific	34%	28%	28%	29%	29%	30%	30%	30%	27%
	Atlantic	24%	25%	24%	26%	24%	27%	27%	28%	27%
L-O3, %sum R in top 10%	Global	35%	35%	33%	35%	36%	36%	36%	36%	36%
	Pacific	33%	32%	29%	32%	31%	32%	32%	32%	32%
	Atlantic	28%	30%	29%	30%	34%	30%	30%	30%	29%
L-CH4, %sum R in top 10%	Global	33%	30%	27%	31%	31%	32%	32%	32%	30%
	Pacific	32%	28%	26%	29%	29%	29%	29%	29%	27%
	Atlantic	27%	25%	21%	26%	27%	27%	27%	27%	25%

992

Global includes all ATom-1 parcels, Pacific considers all measurements over the Pacific Ocean from 53°S to 60°N, and Atlantic uses parcels from 53° S to 60° N over the Atlantic Ocean. All parcels are weighted inversely by the number of parcels in each 10° latitude by 100 hPa bin, and by cosine(latitude). Results from MDS-0 are shown because we have results from six models. Results from the updated MDS-2b are shown (UCIZ*) using the using the current UCI CTM model UCIZ and the RDS* protocol that preprocesses the MDS-2b initializations with a 24 h decay of HNO4 and PAN according to their local thermal decomposition frequencies, see text. See additional statistics in Table S8.

993

Table 3. Cross-model RMS differences (RMSDs as % of mean) for the three reactivities using MDS-0.

P-O3	F0AM	GC	GISS	GMI	NCAR	UCI
F0AM		48%	95%	45%	55%	42%
GC	48%		78%	26%	42%	32%
GISS	95%	78%		81%	72%	75%
GMI	45%	26%	81%		40%	35%
NCAR	55%	42%	72%	40%		42%
UCI	42%	32%	75%	35%	42%	(10%)
L-O3						
F0AM		40%	44%	43%	76%	38%
GC	40%		33%	25%	60%	24%
GISS	44%	33%		36%	66%	30%
GMI	43%	25%	36%		62%	28%
NCAR	76%	60%	66%	62%		60%
UCI	38%	24%	30%	28%	60%	(11%)
L-CH4						
F0AM		47%	136%	48%	82%	45%
GC	47%		111%	20%	60%	27%
GISS	136%	111%		114%	110%	121%
GMI	48%	20%	114%		57%	30%
NCAR	82%	60%	110%	57%		68%
UCI	45%	27%	121%	30%	68%	(14%)

Matrices are symmetric. Calculated with the 31,376 MDS-0 unweighted ATom-1 parcels using the standard RDS protocol. F0AM lacks 5,510 of these parcels because there are no reported J-values. UCI shows RMSD between years 2016 (default) and 1997 as the value in parentheses on diagonal. The unweighted mean R from 3 core models (GC, GMI, UCI) are: P-O3 = 1.97, L-O3 = 1.50, L-CH4 = 0.66, all ppb/d. The three core-model RMSDs with respect to one another are less than 36% and boldened.

994

995

Table 4. ATom data files used here		
Primary Aircraft Data	Formatting and content	Comments
(a) Mor.all.at1234.2020-05-27.tbl (b) Mor.WAS.all.at1234.2020-05-27.tbl (c) Mor.TOGA.all.at1234.2020-05-27.tbl All from Wofsy et al., 2018.	(a) 149133 records x 675 csv columns, 10 s merges of flight data plus chemistry & environmental measurements (b) 6991 records x 729 csv columns, 30-120 s intervals to fill flasks (c) 12168 records x 727 csv columns, 35 s intervals of instrument	Core source of ATom measurements. irregular and difficult formatting; extremely long ascii records; large negative integers or 'NA' for some non-data.
Modeling Data Stream (MDS-2b)		
(a) ATom_MDS2b.nc	(a) netcdf file containing regularly spaced 10 s observations for ATom-1 (32383 records), ATom-2 (33424 records), ATom-3 (40176 records), ATom-4 (40511 records), 146,494 in total; includes physical flight data (11), chemical data (39), miscellaneous data including corrected HNO ₄ and PAN (6), flag data (50).	Regular formatting; all data gap filled with flags to identify the method and extent of filling; NaN's only for flight 46; for use in modeling of the chemistry and related statistics from the ATom 10 s data.
Reactivity Data Stream (RDS-2b)		
(a) ATom_RDS2b.nc	(a) netcdf file containing regularly spaced reactivities for 10 s parcels from ATom-1234 (146,494 in total); includes latitude, longitude and pressure of model grid cell used in the calculation; includes P-O ₃ , L-O ₃ , L-CH ₄ , L-CO, J-O ₁ D, plus dO ₃ /dt = net O ₃ change over 24 h. Reactivities are given for 5 days separated by 5 days in the middle of each deployment, plus the 5-day mean.	Results from newest UCI CTM version (UCIZ) run with RDS* protocol (PAN and HNO ₄ decay) and using MDS-2b. NaN's only for flight 46.